Journal Pre-proofs

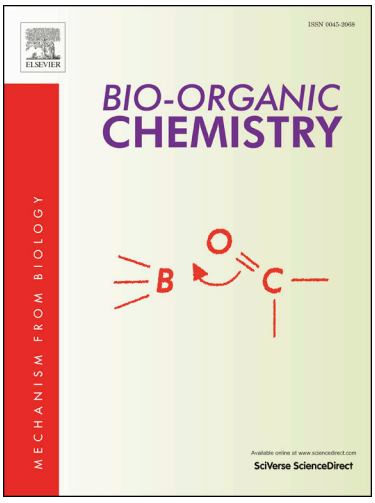

Pyridylethanol(phenylethyl)amines are Non-Azole, Highly Selective *Candida albicans* Sterol 14α-demethylase Inhibitors

Iza Ogris, Urška Zelenko, Izidor Sosič, Martina Gobec, Cene Skubic, Marija Ivanov, Marina Soković, Darko Kocjan, Damjana Rozman, Simona Golič Grdadolnik

PII: S0045-2068(20)31770-3
DOI: https://doi.org/10.1016/j.bioorg.2020.104472
Reference: YBIOO 104472

To appear in: *Bioorganic Chemistry*

Received Date: 12 October 2020
Accepted Date: 10 November 2020

Please cite this article as: I. Ogris, U. Zelenko, I. Sosič, M. Gobec, C. Skubic, M. Ivanov, M. Soković, D. Kocjan, D. Rozman, S. Golič Grdadolnik, Pyridylethanol(phenylethyl)amines are Non-Azole, Highly Selective *Candida albicans* Sterol 14α-demethylase Inhibitors, *Bioorganic Chemistry* (2020), doi: https://doi.org/10.1016/j.bioorg.2020.104472

This is a PDF file of an article that has undergone enhancements after acceptance, such as the addition of a cover page and metadata, and formatting for readability, but it is not yet the definitive version of record. This version will undergo additional copyediting, typesetting and review before it is published in its final form, but we are providing this version to give early visibility of the article. Please note that, during the production process, errors may be discovered which could affect the content, and all legal disclaimers that apply to the journal pertain.

© 2020 Published by Elsevier Inc.

Journal Pre-proofs

Pyridylethanol(phenylethyl)amines are Non-Azole, Highly Selective *Candida albicans* Sterol 14α-demethylase Inhibitors

Iza Ogris [a#], *Urška Zelenko* [a#‡], *Izidor Sosič* [b#], *Martina Gobec* [b], *Cene Skubic* [c], *Marija Ivanov* [d], *Marina Soković* [d], *Darko Kocjan* [a], *Damjana Rozman* [c], *and Simona Golič Grdadolnik* [a*]

[a]Laboratory for Molecular Structural Dynamics, Theory department, National Institute of Chemistry, Hajdrihova 19, 1001 Ljubljana, Slovenia

[b]Faculty of Pharmacy, University of Ljubljana, Aškerčeva 7, 1000 Ljubljana, Slovenia

[c]Center for Functional Genomics and Bio-Chips, Institute of Biochemistry, Faculty of Medicine, University of Ljubljana, 1000 Ljubljana, Slovenia

[d]Institute for Biological Research "Siniša Stanković"- National Institute of Republic of Serbia, University of Belgrade, Bulevar Despota Stefana 142, 11000 Belgrade, Serbia

‡ Present address: Pavčkova ulica 3, 8000 Novo mesto, Slovenia

[#] These authors contributed equally to this work.

*Corresponding Author: Phone: +386 1 4760 409. Fax: +386 1 4760 300.

Email: simona.grdadolnik@ki.si

Journal Pre-proofs

ABSTRACT

Sterol 14α-demethylase (CYP51) is the main drug target for the treatment of fungal infections. The worldwide increase in the incidence of opportunistic fungal infections and the emerging resistance to available azole-based antifungal drugs, raise the need to develop structurally distinct and selective fungal CYP51 inhibitors. In this work we have, for the first time, investigated the binding of pyridylethanol(phenylethyl)amines to any fungal CYP51. The comparison of the binding to *Candida albicans* and human CYP51 studied by spectroscopic and modeling methods revealed moieties decisive for selectivity and potency and resulted in the development of highly selective derivatives with significantly increased inhibitory potency. The structure-based insight into the selectivity requirements of this new chemical class of fungal CYP51 inhibitors, their unique binding properties and the low molecular weight of lead derivatives offer novel directions for the targeted development of antifungal clinical candidates.

Keywords: sterol 14α-demethylase, pyridylethanol(phenylethyl)amines, ligand-receptor interactions, selective *Candida* inhibitors, lead design

Journal Pre-proofs

1. INTRODUCTION

Sterol 14α-demethylase (CYP51) belongs to the cytochrome P450 superfamily. It is a crucial enzyme in the sterol biosynthetic pathway, where it catalyzes the oxidative removal of the 14α-methyl group from sterol precursors. CYP51 has a high substrate specificity with only five naturally occurring, structurally similar 14α-methylsterols as substrates [1]. While prokaryotic CYP51s are soluble proteins, eukaryotic ones are membrane-bound. The final products of sterol biosynthesis are essential structural components of eukaryotic membranes: cholesterol in animals, ergosterol in fungi, and phytosterols in plants. The essential nature of sterol biosynthesis makes CYP51 an important target for drugs to treat infections in humans, animals and plants [2, 3]. For the treatment of human infections, selectivity towards microbial or fungal CYP51 is of crucial importance, since co-inhibition of human CYP51 (hCYP51) would result in the inhibition of cholesterol synthesis and an uncontrolled accumulation of toxic sterols. In the mouse, inactivation of the liver CYP51 enzyme leads to an accumulation of lanosterol and 24,25-dehydrolanosterol and to progressive liver pathology [4, 5]. Due to the potentially toxic effect of sterols and their ability to activate nuclear receptors [6], several drugs targeting this biosynthetic pathway in humans have been discontinued [7] and more attention has been paid to the use of such drug candidates in microbial systems.

Azoles are the most broadly known CYP51 inhibitors and the most widely used antifungals in clinical medicine and agriculture. The supposed basis for the efficacy and safety of azoles is their selective inhibition of fungal CYP51 over the human ortholog. However, measurements of enzyme inhibition on the purified hCYP51 and *Candida albicans* CYP51 (CaCYP51) showed that the selectivity of clinical imidazole ketoconazole and triazole itraconazole is an order of magnitude lower than expected based on previous measurements on microsomal preparations, the difference of the binding affinity is actually less than 10-fold [8]. In general, the triazoles have an improved affinity for fungal over mammalian P450 enzymes compared to the imidazoles. Therefore, clinical triazoles (itraconazole, fluconazole, voriconazole, posaconazole and isavuconazole) have broad application in antifungal therapy whereas for Ketoconazole treatment of systemic human infections is limited [9, 10].

The three-dimensional structures of the CYP51 proteins across biological kingdoms are highly similar despite the low primary sequence identities that can be as low as 22-30 %. The most characteristic feature of the CYP51 structure is the rigidity of the substrate binding cavity, which together with highly similar general fold probably helps to maintain their strictly specific three-step catalytic reaction [2]. First crystal structures of eukaryotic CYP51

were determined for *N*-truncated enzymes [2, 11-14]. In 2014, the first complete crystal structure of the eukaryotic wild type CYP51 from *Saccharomyces cerevisiae* was resolved [15], demonstrating that the entrance into the CYP51 substrate access channel is embedded into the endoplasmic reticulum membrane, with sterol substrates entering through the membrane. In 2017, the crystal structure of *N*-truncated CaCYP51 [16] was solved from a pathogenic *C. albicans*. All structures are highly similar with a typical P450 fold, which consists mainly of α-helices [17]. No major rearrangements in the structures are observed upon ligand binding [10, 14-16]. On the one hand, the stiffness of the active site cavity of CYP51 and the absence of ligand-induced conformational changes allow the design of potent inhibitors with novel molecular scaffolds using the available CYP51 crystal structures in the PDB. On the other hand, the high similarity of human and fungal CYP51 structures makes the development of selective fungal inhibitors a difficult medicinal chemistry task.

As the number of immunocompromised patients, including AIDS and cancer patients, recipients of organ and bone marrow transplants and others receiving immunosuppressive drugs increases, the number of opportunistic fungal infections is emerging. Mortality rates of severe opportunistic fungal infections remain high, e.g. 30-50% for *Candida* species and over 50% for *Aspergillus* species [18]. Prolonged and prophylactic use of azoles results in inhibition of other human P450 enzymes and may lead to drug resistance due to the overexpression of efflux transporters and mutations in the fungal *CYP51* gene leading to its overexpression [19]. The need to develop structurally distinct and selective inhibitors of fungal CYP51 is therefore increasing.

The main goal of this study was the development of potent, structurally distinct CaCYP51 inhibitors with high selectivity against the human ortholog. By applying UV-visible spectroscopy and determining the apparent dissociation constants we identified selective inhibitors of CaCYP51 within a group of pyridylethanol(phenylethyl)amines. Then we used a combination of NMR and molecular dynamics (MD) simulations to gain insight into the binding of these inherently flexible compounds to fungal and human CYP51 orthologs at the atomic level. These two techniques allow the study of dynamic processes in ligand-receptor complexes, which cannot be identified in rigid crystal structures but may affect ligand binding and biological activity. During the investigation of the structural requirements for their selectivity, a number of improved derivatives were designed and synthesized. The binding affinities and inhibitory activities of novel derivatives to fungal ortholog and their selectivity over human ortholog were significantly increased while maintaining their low molecular weight. The pharmacological potential of the most active and selective CaCYP51 inhibitors

was demonstrated by showing antifungal activity towards different *Candida* strains with negligible cytotoxicity on human cells.

2. RESULTS AND DISCUSSION

2.1. Pyridylethanol(phenylethyl)amines are CaCYP51 inhibitors.

It was shown that pyridylethanol(phenylethyl)amines inhibit hCYP51 by coordinating to the heme iron through the pyridine nitrogen [20]; however, their further development as hypolipidemic drugs for the use in humans was hampered by the possibility that toxic sterols could accumulate in some tissues, particularly in the liver. Given that the active sites cavities of hCYP51 and CaCYP51 are structurally very similar, we investigated the potential of these compounds for the development of antifungal lead compounds. Therefore, for the first time, the binding of a group of pyridylethanol(phenylethyl)amines **1**-**10** (Table 1) to any fungal CYP51 was investigated and compared with their binding to the human ortholog.

Spectral responses of type II with peaks at 428-429 nm and troughs at 408-411 nm were produced upon binding of derivatives **1**-**10** to hCYP51 and CaCYP51 (Figure S1). The Soret maximum in the absolute spectrum of the resulting CYP51-inhibitor complexes shifted to 422-423 nm. This was caused by the coordination of pyridine nitrogen to the sixth position of the heme iron [20]. The apparent dissociation constants (K_D) were evaluated by spectral titration to the purified proteins. The K_D of **1** to hCYP51 was previously determined [21]. The K_D values of the clinical azoles, ketoconazole and fluconazole available in the literature [22, 23] are given as a reference. The ketoconazole is recognized as a non-selective CaCYP51 inhibitor, while the fluconazole is one of the most selective CaCYP51 inhibitors over human ortholog [22, 23].

Journal Pre-proofs

Table 1. Apparent dissociation constants (K_D) for the binding of ketoconazole, fluconazole and pyridylethanol(phenylethyl)amine derivatives to hCYP51 and CaCYP51 and the ratio between K_D of hCYP51 and CaCYP51 (S). The experiments were performed in triplicate, and the results are presented as means ± SD.

Compound		K_D (μM)		S
		CaCYP51	hCYP51	
Ketoconazole	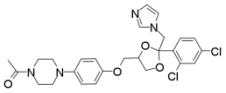	0.012 ± 0.003[a]	0.061 ± 0.017[a]	5.1
Fluconazole	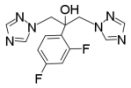	0.056 ± 0.004[a]	30.5 ± 7.7[a]	543
1	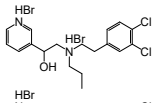	0.31 ± 0.03	0.13 ± 0.03[b]	0.4
2	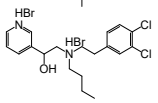	0.49 ± 0.04	0.45 ± 0.01	0.9
3	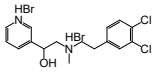	8.5 ± 0.7	6.1 ± 0.7	0.7
4	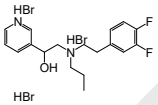	0.54 ± 0.07	13 ± 1	24
5	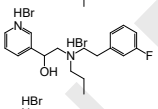	6.9 ± 0.4	26 ± 1	3.8
6	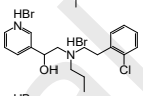	0.32 ± 0.07	35 ± 2	109
7	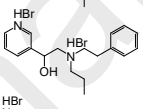	1.8 ± 0.1	80 ± 6	44
8	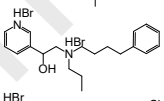	4.6 ± 0.2	4.0 ± 0.2	0.9
9	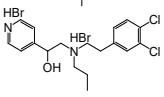	0.33 ± 0.07	3.2 ± 0.1	9.7
10	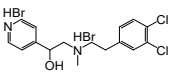	6.9 ± 0.5	20 ± 1	2.9

[a]Published by Warillow et al. [23]
[b]Published by Zelenko et al. [21]

The comparison of K_D for binding to hCYP51 and CaCYP51 of derivatives **1**-**10** (Table 1) reveals that the substitution pattern on the phenyl ring is the most important factor influencing the selectivity of these compounds by changing the binding affinity to hCYP51 by one or two orders of magnitude. At the same time, variations of the phenyl ring substituents do not affect the binding to CaCYP51. The most notable selectivity ratio was determined for compounds

with 2-chloro-substituted (**6**) and unsubstituted (**7**) phenyl ring (Table 1). The binding of these two compounds to hCYP51 was reduced by two orders of magnitude compared to **1**, whereas **6** bound with similar and **7** with slightly reduced binding affinity to CaCYP51 as compound **1**. The 3,4-dichloro substitution pattern of the phenyl ring is detrimental for selectivity because the affinity for hCYP51 and CaCYP51 did not differ for compounds **1**, **2**, and **3**, which vary only in the length of an alkyl chain. Interestingly, the replacement of the two Cl atoms by F atoms caused a gain in selectivity, as evident with **4** (Table 1). The 3-monofluoro substitution of the phenyl ring (**5**) weakened binding to both CaCYP51 and hCYP51 and had no notable effect on selectivity. The length of the alkyl chain had no effect on selectivity, but it is important for the binding to both CaCYP51 and hCYP51. The extension of this substituent generally led to an increase in binding affinity (Table 1). Other structural features, such as a change in the position of the pyridine nitrogen (**9** and **10**) or an increased length of the alkyl chain connecting the phenyl ring with the tertiary amine nitrogen (**8**), had no notable effect on selectivity. The affinities of these three compounds to CaCYP51 were also not increased compared to compound **1** (Table 1).

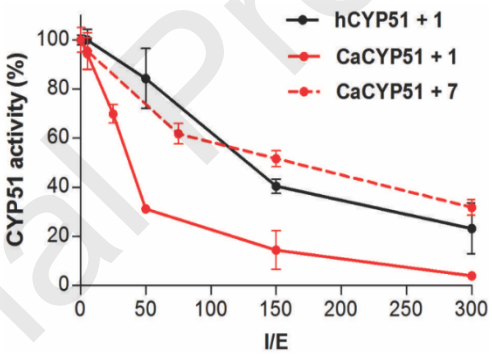

Figure 1. Inhibitory potencies of **1** and **7** on CaCYP51 and hCYP51 in a 30-minute reaction at 37 °C. The CYP51 concentration was 1 µM and the enzyme/substrate molar ratio was 1/50. The experiments were performed in triplicate, and the results are presented as means ± SD.

The best non-selective CaCYP51 binder **1** and the selective binder **7** with the lowest affinity for hCYP51 were chosen to confirm inhibition potency and selectivity by testing the activity of CaCYP51 and hCYP51 *in vitro* using radiolabeled [3-^{3}H]-lanosterol as described in the literature [23, 24]. In this inhibition assay, both CYP51 orthologs were inhibited by **1** (Figure 1). The molar ratio of inhibitor/enzyme (I/E) required for a 2-fold decrease in CYP51 activity was 37 µM for CaCYP51 and 128 µM for hCYP51. On the contrary, derivative **7** only

inhibited CaCYP51 (I/E ~ 140 μM) and concurrently showed no inhibition of human CYP51, even if the I/E was up to 5000/1 (Figure 1). These results show that pyridylethanol(phenylethyl)amines have a potential for the development of selective fungal inhibitors.

2.2. Structural insight into the selectivity requirements of pyridylethanol(phenylethyl)amines.

We have already shown that the combination of ligand-based NMR methods and molecular modeling can provide insight into the binding mode of these inherently flexible derivatives at the atomic level. The binding mode of compound **1** in hCYP51 was determined, revealing its unique binding properties [21]. Most importantly, it has been shown that the halogenated phenyl ring of **1**, which is the only common moiety with the azoles, is not located in the hydrophobic channel near the pyrrole ring D of heme, as in the crystal structures of the azoles in complex with CYP51 orthologs. Instead, it is located in the substrate access channel, where it exhibits a unique series of interactions compared to the azoles [21].

Transferred NOESY (trNOESY) spectra (Figure 2) indicated that bound conformations of **1** in CaCYP51 are similar to those in hCYP51. Mutually exclusive NOEs of the H7' proton with the H2" protons in the propyl chain and with the H7 protons in the phenethyl fragment, which typically indicate the existence of the two diastereomeric forms of these compounds [25], were observed in the presence of both CYP51 orthologs (Figure 2, blue arrows). A diastereomeric effect in these compounds is the consequence of a dynamic process consisting of acid dissociation, nitrogen inversion, nitrogen reprotonation, and conformational reorganization [25]. *RS* (*SR*) and *RR* (*SS*) diastereomeric pairs have a different steric position of the H7' proton relative to the propyl chain and the phenethyl moiety [25], which is retained in the active site of the two CYP51 orthologs. The two-letter code for the stereochemical designation pertains to the chiral hydroxyl bound carbon C7' (first letter) and the protonated tertiary amine nitrogen (second letter). The NOEs between the alkyl chain protons H2" and H3" with the H2 in the pyridine ring (Figure 2, orange arrows) and the H2' in the halogenated phenyl ring (Figure 2, red arrows) were also observed in both cases. It was shown that these NOEs indicate multiple locations of the propyl chain [21], which can adapt to various hydrophobic regions within the active site cavity by establishing spatial contacts with either pyridine (Figure 2, orange arrows) or phenyl (Figure 2, red arrows) rings. The aromatic ring moieties, on the other hand, are firmly positioned in their binding pockets regardless of the

location of the propyl chain [21]. Since the pyridyl nitrogen of these derivatives is coordinated to the heme iron, as revealed by UV-visible spectroscopy, the absence of NOEs between the aromatic rings in the presence of CaCYP51 or hCYP51 (Figure 2) defines the position of the halogenated phenyl ring in the substrate access channel of each ortholog. The identical NOE pattern in the presence of CaCYP51 or hCYP51 revealed the common position of the ligand moieties in their active sites.

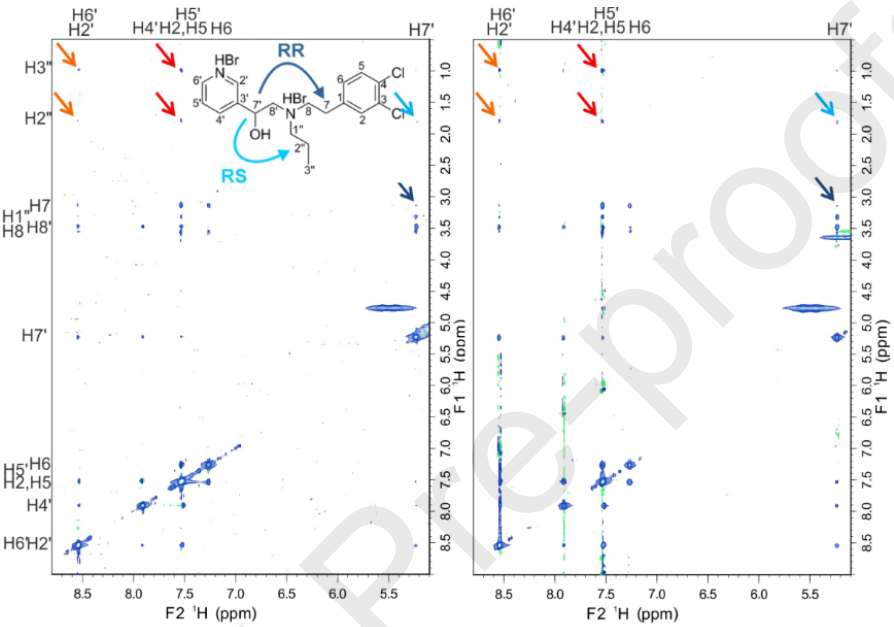

Figure 2. Expanded regions of the trNOESY spectrum of **1** in the presence of hCYP51 (left) and CaCYP51 (right) recorded at 800 MHz with the structure of **1** illustrating the atom nomenclature and typical NOE connectives of *RS* and *RR* diastereomers. Weak NOE connectivities are clearly visible in the 1D traces. The crucial NOE connectivities are marked with colored arrows (the H7' - H2" with light blue, the H7' - H7 with dark blue, the H2' - H2" and the H2'-H3" with orange, and the H2 - H2" and the H2 - H3" with red).

The extensive unrestrained MD simulations of the non-selective derivative **1** and the selective derivatives **6** and **7** in the complex with CaCYP51 and hCYP51 were performed to get structural insights into the selectivity requirements. All four diastereomers of each of the three derivatives adopt matching binding poses in either CaCYP51 or hCYP51 (Figure S7). Therefore, only *RS* diastereomers were selected for further comparison of the specific ligand contacts with the two CYP51 orthologs.

In the MD simulations, no major rearrangements in the CaCYP51 and hCYP51 structures were observed upon binding of **1**, **6**, and **7** with respect to the crystal structures of CaCYP51

in complex with VT-1161 (PDB entry 5TZ1) [16] and the crystal structure of hCYP51 in complex with ketoconazole (PDB entry 3LD6) [14], respectively. The root mean square deviations (RMSD) are provided in Table S2. The phenyl ring of all three derivatives had a similar disposition in the substrate access channel in either CaCYP51 or hCYP51 (Figure 3). The ligand-protein interaction energy was dominated by the Lennard-Jones contribution (Tables S3, S4 and S5). With the exception of **7** in complex with hCYP51, the complexes were stable during the MD simulations (Figure S8). Compound **7** had a significantly lower binding affinity to hCYP51 in comparison to other derivatives (Table 1).

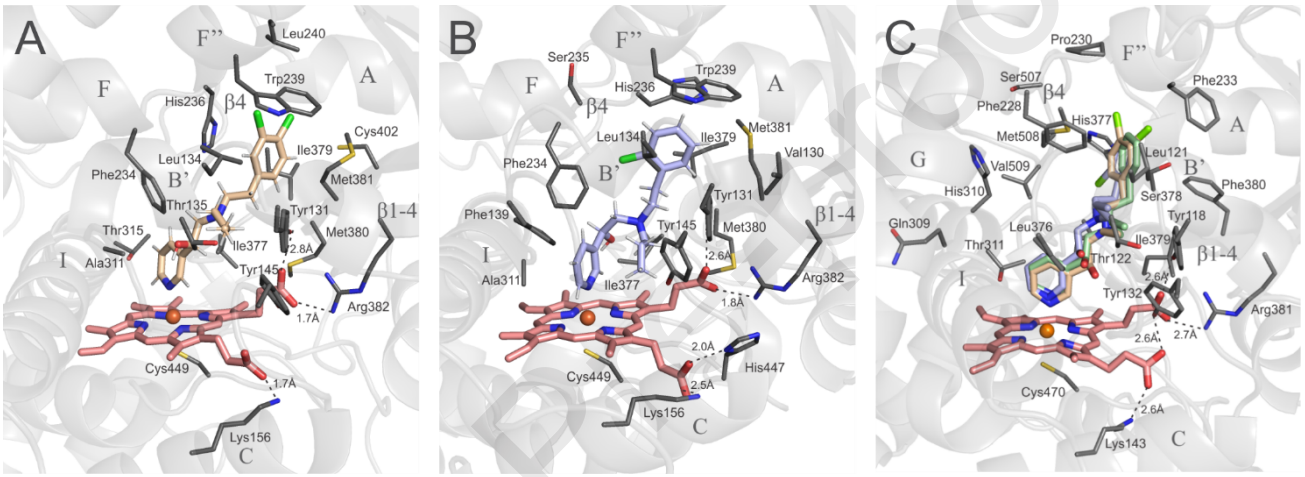

Figure 3. Snapshots from the MD trajectories showing: (A) the binding pose of derivative **1** in the active site of hCYP51; (B) the binding pose of derivative **6** in the active site of hCYP51; (C) comparison of binding poses of **1** (in brown), **6** (in violet), and **7** (in green) in active site of CaCYP51. The amino acids within 4.5 Å of the compounds and the amino acids that form hydrogen bonds (black dashes) with heme propionates are labeled. The secondary structure elements are shown as cartoon.

The active site cavity of CYP51 is bordered by the heme, B' helix/B'C loop, the *N*-terminal parts of helices C and I, β1-4 strand with the preceding K'/β1-4 loop and β4 hairpin. The entrance into the substrate access channel is formed by the helices A', F'' and β4 hairpin on the upper side of the protein. CaCYP51 and hCYP51 have a similar FG loop containing the helix F" at the top of the access channel. Upon substrate binding, the FG loop moves downwards and the helix F" closes the entrance to the substrate access channel, while this entrance is open in the ligand-free and inhibitor-bound CYP51 state [26, 27]. Nevertheless, the indole ring of Trp239 within the F" helix forms a lid in the hCYP51 substrate access

channel, even in the ligand-free or ligand-bound hCYP51 state [14], making its entrance narrower compared to CaCYP51 (Figure 3).

In general, five amino acids form hydrogen bonds with the heme propionate side chains [28, 29]. It has been suggested that the ability of the ligands to break the hydrogen bonds between heme and tyrosines (Tyr131, Tyr145 in hCYP51 and Tyr118, Tyr132 in CaCYP51) probably contributes to their inhibitory efficacy and may also be responsible for their selectivity because in many protozoan CYP51 inhibitor complexes these two hydrogen bonds have been broken [11, 12, 30]. However, the role of these hydrogen bonds in the mechanism of CYP51 inhibition remains an open topic, since they were not disturbed in the crystal structures of azoles in complexes with hCYP51 [14] and CaCYP51 [16].

MD simulations of the CYP51 complexes with **1**, **6** and **7** showed that the inhibitory potency or selectivity of the pyridylethanol(phenylethyl)amines cannot be associated with the hydrogen bonding network of the tyrosines. In the MD trajectories of the hCYP51 complexes with the non-selective derivative **1** and the selective derivative **6,** the hydrogen bond of Tyr131 with heme ring A propionate was retained, while the hydrogen bond of Tyr145 with heme ring D propionate was rarely formed (Figure S9). In the MD trajectories of the CaCYP51 complexes, the hydrogen bonds of Tyr118 and Tyr132 with heme were preserved for all three derivatives (Figure S9).

However, the differences in inhibitory potency and selectivity of **1**, **6,** and **7** can be associated with differences in the specific contacts of their phenyl ring moieties with the residues in the substrate access channel. In the MD trajectories of the hCYP51 complexes, the phenyl moieties were surrounded by Leu134, His236, Trp239, Leu240, Ile379, Met381, and Cys402, with the indole ring of Trp239 forming a lid over the access channel (Figures 3A and 3B). The interaction energy of the 3,4-dichloro substituted phenyl ring of non-selective derivative **1** with the surrounding residues was stronger compared to the 2-chloro substituted phenyl ring of selective derivative **6** (Table S3), which is consistent with the observed differences in the binding affinity of **1** and **6** (Table 1). Furthermore, differences in the interaction energies can be attributed to different substitution patterns of the phenyl rings of **1** and **6**. The 3-Cl and 4-Cl atoms of **1** made numerous contacts with the surrounding residues (Figure 3A). Particularly energetically beneficial were contacts of the 3-Cl atom with His236, Trp239 and contacts of the 4-Cl atom with His236, Ile 379, and Met381 (Table S4). The interaction energy of the 2-Cl atom of **6** with the surrounding residues was less favorable (Table S4). Its interaction energy with the nearby Phe234 was even repulsive.

In CaCYP51 the phenyl moieties of **1**, **6**, and **7** were surrounded by Leu121, Pro230, Phe233, His377, Ser378, Phe380, Ser507, Met508 and Val509 (Figure 3C). Regardless of the position of the Cl atoms, the interaction energies of the phenyl moieties of **1** and **6** with the surrounding residues were comparable (Table S5), as was their binding affinity to CaCYP51 (Table 1). The interaction energy of the unsubstituted phenyl ring of the less potent derivative **7** was significantly lower (Table S5).

Recent crystallographic studies have shown that the binding of azole-based compounds, VFV analogues, to hCYP51 stiffens the enzyme I-helix by restoring the main-chain hydrogen bonds in its loop-like region [31]. These results confirmed the assumption that the loop-like region in the middle part of the I-helix, which is not observed in fungal CYP51, makes the human enzyme more flexible than the fungal one and is, therefore, more resistant to the inhibitor binding.[10, 31] The results of our MD simulations of ligand-hCYP51 complexes showed that pyridylethanol(phenylethyl)amines do not stabilize the I-helix. This can be explained by a different binding mode of these compounds in compassion to azoles. Therefore, a lower number of contacts between the I-helix and **1** and **6** (Figures 3A and 3B) was observed compared to VFV analogues [31] and ketoconazole [14]. In MD simulations of ligand-hCYP51 complexes, the rigidity of the I-helix was released compared to the crystal structure of the ketoconazole-hCYP51 complex [14] (Figure 4A). The loop-like region in the middle part of the I-helix was similar in the complex with the non-selective derivative **1** and the selective derivatives **6** (Figure 4B).

Journal Pre-proofs

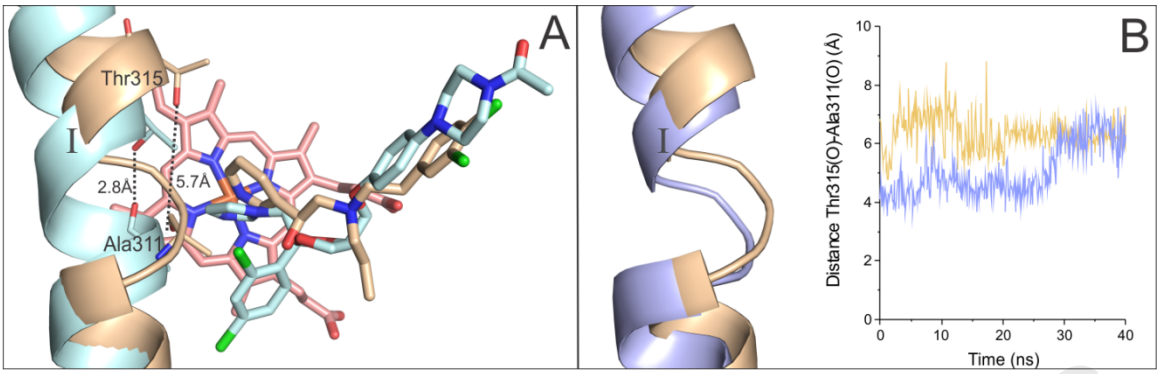

Figure 4. Effect of pyridylethanol(phenylethyl)amines on the structure of the I-helix in hCYP51. (A) Superimposed structures of the ketoconazole - hCYP51 (in cyan, PDB entry 3LD6) [14] and **1** - hCYP51 (in brown, snapshot from MD trajectory) complexes. The distances between the side chain oxygen of Thr315 and the backbone oxygen of Ala311 are given. (B) Snapshots from MD trajectories showing the superposition of the I-helices of hCYP51 in the complex with derivative **1** (in brown) and **6** (in violet). The distances between the side chain oxygen of Thr315 and the backbone oxygen of Ala311 are along MD trajectory are shown.

2.3. Development, synthesis, and specific binding of novel pyridylethanol(phenylethyl)amines.

The first goal of the design of optimized derivatives was to further investigate the most appropriate substitution pattern of the halogenated phenyl ring to enhance selectivity for CaCYP51. Since the derivatives with 3,4-dichloro substituted phenyl ring listed in Table 1 clearly showed no selectivity, this substitution pattern was excluded when designing new derivatives. The 3-mono substituted pattern was also excluded because the binding of compound **5** to CaCYP51 was reduced and no apparent improvement in selectivity over the human orthologue was observed (Table 1). The 2-fluoro, 2-chloro, 3,4-difluoro, and unsubstituted phenyl ring moieties were selected because they led to a substantial increase in the selectivity compared to inhibitors with the 3,4-dichloro substitution pattern (Table 1). The second goal was to optimize the binding to CaCYP51 without compromising selectivity. Therefore, derivatives with the most appropriate phenyl ring substitution patterns in terms of selectivity, but with prolonged alkyl chain, were designed (Table 2). The replacement of the alkyl chain by a bulky substituent was also proposed to investigate the effects of increased bulkiness and possible changes in the conformational flexibility of the bound ligand on ligand

binding affinity. In order to increase the sp3 character of the molecules and to enable a direct comparison of the phenyl-cyclohexyl isosteric replacement on both affinity and selectivity, compound **34** (Scheme S1, Table 2) was prepared.

The synthetic approach towards final compounds is presented in Scheme 1 and S1. All procedures were performed as described previously [25], except for the amide bond reduction in the last step. Here, we used the $NaBH_4$-I_2 system in THF instead of the borane-dimethyl sulfide complex.

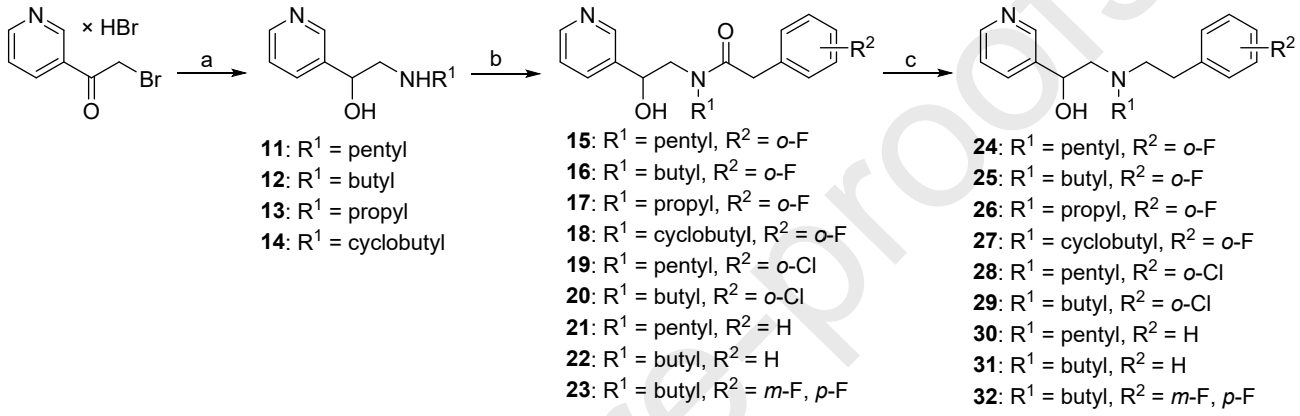

Scheme 1. Reagents and conditions: (a) (i) $NaBH_4$, EtOH, rt, 2 h; (ii) R^1NH_2, EtOH, reflux, 5 h; (b) corresponding phenylacetic acid, EDC, HOBt, CH_2Cl_2, rt, 24 h; (c) $NaBH_4$-I_2, THF, 0 °C to reflux, 24 h.

In analogy to the compounds listed in Table 1, apparent K_D of derivatives **24**-**32** and **34** to hCYP51 and CaCYP51 (Table 2) were determined using the UV-visible spectroscopy (Figure 5). Optimized derivatives showed an improved and more selective binding to CaCYP51. In general, the most selective among the new derivatives were those with the 2-fluoro substituted phenyl ring (**24**, **25** and **26**, Table 2) with a selectivity factor in the range of 300 to 450, an increase for four orders of magnitude compared to **1**. The extension of the alkyl chain was beneficial for the binding to both orthologs and had no significant effect on selectivity. Derivatives with pentyl chain (**24**, **28**, and **30**, Table 2) had a K_D one order of magnitude higher compared to their counterparts with propyl chain (**26** in Table 2, **6** and **7** in Table 1). The increased bulkiness introduced by replacing the alkyl chain with a cyclobutyl ring (**27**) or by replacing the phenyl with a cyclohexyl ring (**34**) was not beneficial for either binding or selectivity.

Table 2. Apparent dissociation constants (K_D) for the binding of newly designed pyridylethanol(phenylethyl)amines to hCYP51 and CaCYP51 and the ratio between K_D of hCYP51 and CaCYP51 (S). The experiments were performed in triplicate, and the results are presented as means ± SD.

Compound		K_D (μM)		S
		CaCYP51	hCYP51	
24	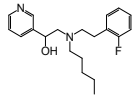	0.027 ± 0.004	8.2 ± 0.6	304
25	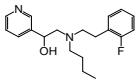	0.088 ± 0.009	40 ± 3	455
26	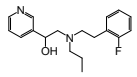	0.24 ± 0.01	76 ± 4	317
27	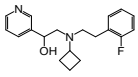	0.45 ± 0.03	119 ± 8	264
28	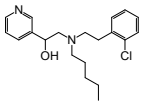	0.014 ± 0.003	4.0 ± 0.2	286
29	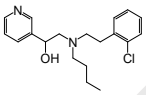	0.11 ± 0.01	20 ± 1	182
30	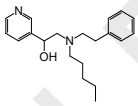	0.069 ± 0.002	10 ± 1	145
31	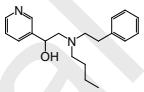	0.36 ± 0.02	71 ± 4	197
32	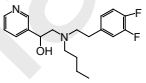	0.42 ± 0.03	6.3 ± 0.6	15
34	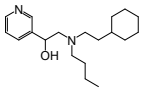	2.2 ± 0.2	61 ± 6	28

The fact that 2-fluoro substitution proved to be the most promising was not entirely surprising since it is known that the strategic incorporation of fluorine into a molecule can affect a range of properties that are crucial for drug design. It has been shown that the introduction of fluorine influences potency, the modulation of hydrophobic interactions, lipophilicity, permeability, and metabolic stability. In addition, it has been shown that fluorine strongly influences the conformational properties of molecules, especially when attached at the ortho position to the linking substituent [32].

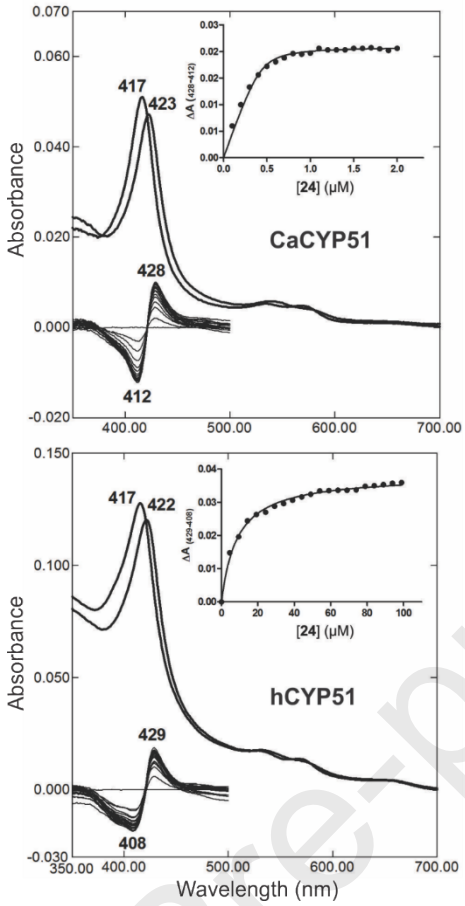

Figure 5. Type II spectral response of CaCYP51 and hCYP51 to the addition of derivative **24**.

2.4. Biological evaluation of selected pyridylethanol(phenylethyl)amines.

The derivatives with 2-fluoro substituted phenyl ring moiety were additionally evaluated in the *in vitro* reconstituted CYP51 reaction. The inhibitory potency was tested on 0.5 μM CYP51 at a molar ratio E/I/S of 1/30/50 after 1 h CYP51 reaction. During this time the conversion of lanosterol into the product follicular fluid-meiosis-activating substance (FF-MAS) without inhibitor was ~95%. The inhibition assay was performed with LC-MS to assess the concentrations of lanosterol and FF-MAS. This method allowed us to avoid the use of the expensive radiolabeled [3-^{3}H]-lanosterol, which is used in the standard CYP51 inhibition assays also applied in Chapter 2.1 for compounds **1** and **7**.[23, 24, 33] Furthermore, for calculation of the substrate conversion with the standard method, where radiolabeled [3-^{3}H]-lanosterol and [3-^{3}H]-FF-MAS are detected, the peaks areas in the radioactivity detector signal are used, which does not necessarily correspond to the concentrations of the analytes. When using a mass spectrometer as a detector, the concentrations of the analytes can be

measured in relation to the concentration standard curves. Therefore, the determination of the lanosterol conversion to FF-MAS as a molar ratio is quantitatively more accurate.

As shown in Figure 6, the strongest potencies against CaCYP51 were shown by derivatives **24** (48%) and **25** (45%), i.e. twice as high as for the selective derivative **6** (21%) from the first series (Table 1). The relative potencies against CaCYP51 of all tested derivatives were consistent with the strength of the apparent K_D values. Ketoconazole and fluconazole were used as positive controls and resulted in 100% inhibition of CaCYP51. No inhibitory effects were detected when derivatives **24**, **25**, **26**, **27**, **6** and **7** were tested against hCYP51 in the same E/I/S ratio. As expected, ketoconazole and the non-selective derivative **1** showed inhibition of hCYP51, 81% and 22%, respectively. Fluconazole, which is known as a selective inhibitor, showed inhibition of 2%. These results further substantiate the high selectivity of the 2-fluoro-substituted phenyl derivatives.

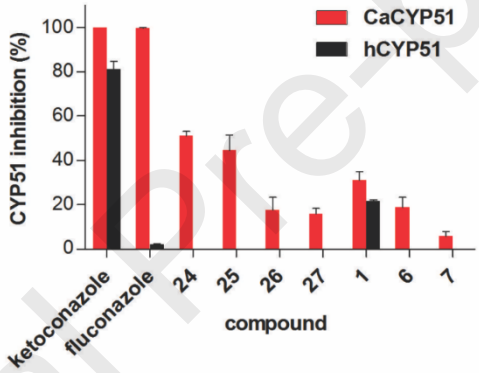

Figure 6. The inhibitory potencies of ketoconazole, fluconazole, **24**, **25**, **26**, **27**, **1**, **6** and **7** were compared as a percentage of inhibition of CaCYP51 and CYP51 in a 60 minute reaction at 37 °C. The CYP51 concentration was 0.5 µM and the molar ratio enzyme/inhibitor/substrate was 1/30/50. The experiments were performed in triplicate, and the results are presented as means ± SD.

The relative differences in the inhibitory effect between stronger and weaker inhibitors were smaller compared to the differences in their K_D values. This type of disparity was also observed in other studies [30, 33, 34] and, as suggested by Lepesheva *et. al.,* lower inhibitory potency could be a result of the protein conformational dynamics associated with substrate recognition, interaction with reductase, electron transfer and subsequent reduction. This could cause a reduced binding cavity and a lower number of contacts between the binding cavity

and the inhibitor. Therefore, the inhibitor can be released more easily from the active site [33].

Finally, the antifungal activity of the selective derivatives with the 2-fluoro substituted phenyl ring was investigated by assessing their activity against different *Candida* (Table 3) *and Aspergillus* strains (Table S1). All compounds were able to inhibit growth of tested *Candida* species with the *Candida glabrata* clinical isolate being most sensitive with minimum inhibitory concentration (MIC) values in the range of 3 to 5 μg/mL. *C. albicans* strains 475/15 and ATCC 10231 and *Candida tropicalis* were most sensitive to treatment with compound **24** (MIC 100 μg/mL)**.** *Aspergillus versicolor* was most sensitive among the *Aspergillus* strains tested with MIC values in the range of 100 to 160 μg/mL (Table S1). Overall, the inhibition of the *Candida* strains by selected derivatives was considerably stronger than the inhibition of the *Aspergillus* strains.

Table 3. Antifungal activity of selected pyridylethanol(phanylethyl)amines and clinical azoles ketoconazole and fluconazole (MIC ± SD μg/mL) against *Candida* strains. Different letters in each column indicate a significant statistical difference between the samples ($p < 0.05$).

Compound	*C. glabrata* 4/6/15	*C. albicans* 475/15	*C. krusei* H1/16	*C. albicans* ATCC 10231	*C. tropicalis* ATCC 750	*C. parapsilosis* ATCC 22019
24	3 ± 0.05^{c}	100 ± 1^{c}	200 ± 3^{b}	100 ± 1^{c}	100 ± 1^{c}	100 ± 2^{c}
25	3 ± 0.05^{c}	200 ± 3^{d}	200 ± 3^{b}	200 ± 4^{e}	400 ± 4^{e}	100 ± 1^{c}
26	5 ± 0.08^{d}	320 ± 2^{e}	320 ± 2^{c}	160 ± 2^{d}	320 ± 4^{d}	160 ± 1^{d}
27	5.4 ± 0.04^{d}	340 ± 2^{e}	1360 ± 0.01^{d}	680 ± 4^{f}	1360 ± 10^{f}	/
Ketoconazole	1.6 ± 0.01^{b}	3.1 ± 0.02^{b}	1.6 ± 0.01^{a}	1.6 ± 0.01^{b}	1.6 ± 0.01^{a}	3.1 ± 0.02^{b}
Fluconazole	0.5 ± 0.01^{a}	1 ± 0.02^{a}	/	0.5 ± 0.01^{a}	2 ± 0.02^{b}	0.5 ± 0.01^{a}

To exclude the possibility that the antifungal activity is caused by non-specific cytotoxic effects, derivatives **24**, **25**, **26**, and **27** were evaluated on human peripheral blood mononuclear cells (PBMC) (Figure 7). As shown in Figure 7, these derivatives had no pronounced effect on the viability of PBMCs.

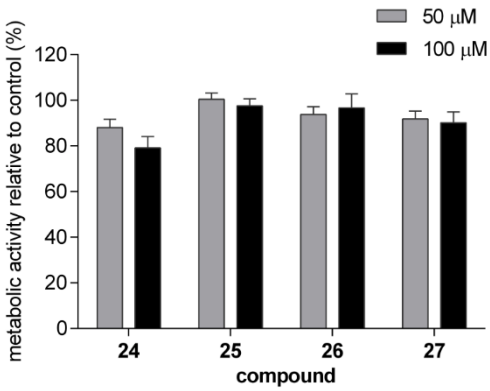

Figure 7. Cytotoxic effects of derivatives **24**, **25**, **26**, and **27** on human peripheral blood mononuclear cells. The results are expressed as a percentage in relation to the control after 24 h exposure to the compounds. The data represent three independent biological experiments and presented as means ± SD.

The biological evaluation presented herein yielded compound **24** as the most promising representative of a novel chemical class of selective CaCYP51 inhibitors.

2.5. Structural insight into the binding properties of compound 24 in CaCYP51.

The increased length of the alkyl chain of **24** did not restrict its location in the active site. In the trNOESY spectra of **24** in the presence of CaCYP51, the same NOE pattern was observed (Figure S5) as for the other derivatives. The pentyl chain showed NOEs with protons of pyridine and phenyl rings, indicating multiple locations of the chain in the active site. However, the ligand epitope maps obtained by 1D saturation transfer difference (STD) NMR [35] of **24** compared to **25** and **26** clearly show a relative increase in the strength of the interaction between the chain and the enzyme (Figure 8).

The unrestrained MD simulations of derivatives **24, 25,** and **26** in complex with CaCYP51 also showed a correlation between the magnitude of the interaction energy of the alkyl chain with the enzyme and its length (Figure 9). Interestingly, a stronger interaction of the longer alkyl chain is also beneficial for the interactions of the 2-fluoro substituted phenyl ring with the enzyme (Table S6). The 2-fluoro substituted phenyl ring of **24** reached the channel entrance gated by the helices A', F'' and β4 hairpin (Figure 10A) and established contacts with Tyr64 (A' helix), Ser507, Met508 (β4 hairpin), Tyr118 (B' helix), Leu376, His377, Ser378 (K helix/β4 loop), and Phe380 (β1-4 strand). The pentyl chain was located in the region bordered by the helices B' and F" and the F- F" loop and made contacts with Ala117, Tyr118, Leu121, Thr122, (B' helix), Phe230, Phe233 (F" helix), Phe380 (β1-4 strand), and

Met508 (β4 hairpin). The hydrogen bonds of Tyr118 and Tyr132 with heme were formed during the MD simulations (Figure S10).

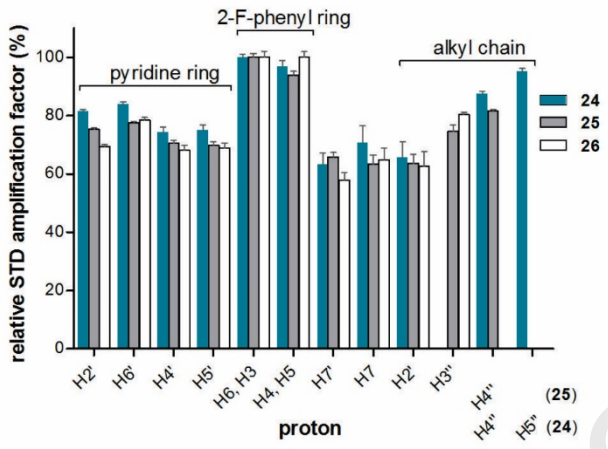

Figure 8. Relative degrees of saturation of the individual protons of the derivatives **24** (in cyan), **25** (in gray), and **26** (in white), determined from 1D STD NMR spectra recorded at a CaCYP51/ligand ratio of 1:100 and 600 MHz (Figure S6). The values in each molecule were normalized to the intensity of the signal with the largest STD effect. The signals of the protons not shown were overlapped with the buffer signals in the reference experiment. The proton nomenclature corresponds to the atom nomenclature shown in Figure 2 and Figure S6.

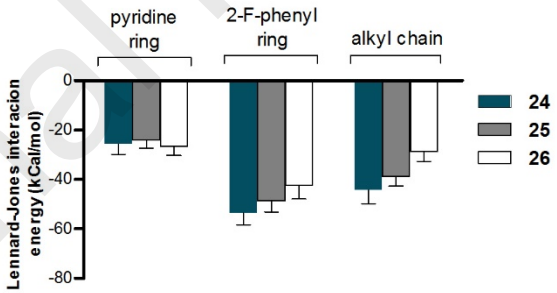

Figure 9. Lennard-Jones interaction energy during the MD simulation of the alkyl chain, the 2-fluoro substituted phenyl ring, and the pyridine ring moieties of derivatives **24, 25,** and **26** with CaCYP51. The average energies and their RMSD deviations over the trajectory are shown.

The investigated pyridylethanol(phenylethyl)amines, including compound **24**, have a different binding mode to hCYP51 and CaCYP51 than the azoles (Figure 10B). The halogenated ring, which is the most important moiety of this class to achieve selectivity towards CaCYP51, is located in the substrate access channel. In CYP51 complexes with

azoles, which typically branch into the Y-shape [14-16], the halogenated phenyl ring extends into the hydrophobic channel near the pyrrole ring and its elongated tail extends into the substrate access channel.

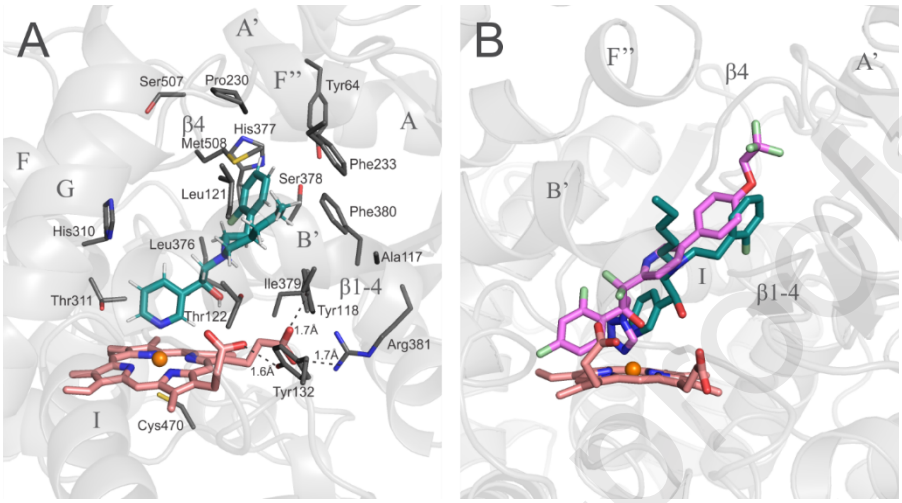

Figure 10. (A) The snapshot from the MD trajectory showing the binding pose of compound **24** in the active site of CaCYP51. The amino acids within 4.5 Å of 24 and the amino acids Tyr-132, Tyr-118, and Arg-381 which form hydrogen bonds (black dashes) with heme propionates are labeled. The secondary structure elements are shown as cartoon. (B) Comparison of the binding mode of **24** (in cyan) and azole VT-1161/oteseconazole (in pink, crystal structure PDB entry 5TZ1) [16].

3. CONCLUSIONS

The increasing resistance to currently available therapeutic options for fungal infections highlights the need to develop new classes of CYP51 inhibitors with antifungal activity. In this study, we have described a focused library of highly selective fungal CYP51 inhibitors with unique binding positions resulted in potent and highly selective CaCYP51 inhibitors of the pyridylethanol(phenylethyl)amine class. The most potent derivatives were further biochemically characterized and their binding was evaluated using NMR and MD techniques. The extensive study yielded compound **24** as the most promising representative of this chemical class of CaCYP51 inhibitors.

The low molecular weight of the designed compounds and in-depth studies on their binding offer numerous options for further optimization. We are confident that the discovery of these compounds will pave the way toward even more potent and selective second-generation inhibitors. We also believe that the scientific community will consider the represented information as an opportunity to use compound **24** as a starting point for focused lead optimization that could eventually furnish structurally novel antifungals with clinical candidate potential.

4. EXPERIMENTAL SECTION

4.1. Chemistry.

General Methods. Reagents and solvents were obtained from commercial sources (i.e., Acros Organics, Aldrich, TCI Europe, Merck, Alfa Aesar, Fluorochem). Solvents were distilled before use, while the other chemicals were used as received. Reactions were monitored using analytical thin-layer chromatography plates (Merck 60 F254, 0.20 mm), and the components were visualized under UV light and/or through staining with the relevant reagent. Flash column chromatography was performed on Merck Silica Gel 60 (particle size 0.040-0.063 mm; Merck, Germany), using the indicated solvents. ^{1}H and ^{13}C NMR spectra were recorded on a Bruker Avance 400 MHz spectrometer at 295 K. The chemical shifts (δ) are reported in parts per million (ppm) and are referenced to the deuterated solvent used. The coupling constants (*J*) are given in Hz, and the splitting patterns are designated as follows: s, singlet; br s, broad singlet; d, doublet; dd, double doublet; ddd, doublet of doublet of doublets; dtd, doublet of triplet of doublets; t, triplet; td, triplet of doublets; dt, doublet of triplets; m, multiplet; symm m, symmetrical multiplet; app, apparent. High-resolution mass measurements were recorded using a Thermo Scientific Q Exactive Plus mass spectrometer. HPLC purity analyses were performed on Thermo Scientific DIONEX UltiMate 3000 instrument equipped with diode array detector using Acquity UPLC® HSS C18 SB column (1.8 μm, 2.1 mm × 50 mm). The mobile phase consisted of 0.1% trifluoroacetic acid in water (A) and acetonitrile (B), employing the following gradient: 95% A to 5% A in 10 min, then 95% B for 4 min, with a flow rate of 0.3 mL/min and injection volume of 5 μL. Column temperature during analysis was 45 °C. The purities of the final derivatives used for the biological evaluations were >95%, as determined by HPLC (unless noted otherwise).

*General procedure for the reduction of amides **15-23** and **33***. In a three-neck round bottom flask, $NaBH_4$ (2.5 equiv.) was suspended in freshly distilled THF (10 mL for 4.5 mmol of $NaBH_4$) at 0 °C. A solution of the corresponding amide (1 equiv.) in freshly distilled THF (5 mL for 2.0 mmol of amide) was added and stirred at 0 °C for 10 min, followed by a dropwise addition of a solution of I_2 (1 equiv.) in freshly distilled THF (5 mL for 2.0 mmol of I_2) via cannula. The reaction mixture was then stirred at reflux for 24 h and quenched by consecutive addition of EtOAc (5 mL), MeOH (5 mL) and H_2SO_4 (2 M, 5 mL) at 0 °C. Volatiles were then evaporated and the remaining aqueous phase alkalized to pH 12 using 2 M NaOH. The aqueous phase was extracted with CH_2Cl_2 (3 × 100 mL), the combined organic layers washed with brine (2 × 100 mL), dried with Na_2SO_4, filtered, and evaporated under reduced pressure. The crude products were purified by flash column chromatography. After purification, selected compounds **24**-**27** were transformed into dihydrobromide salts to ensure greater stability and better aqueous solubility needed for CYP51 inhibition assay, NMR assays, antifungal activity determination, and cytotoxicity evaluation. This was performed by treatment of a solution of free amines in acetone (5 mL) with an excess of 33% HBr in acetic acid at 0 °C, followed by evaporation of solvents, trituration of residues with Et_2O, and filtration.

*2-(Pentylamino)-1-(pyridin-3-yl)ethan-1-ol (**11**).* This compound was purified by flash column chromatography using CH_2Cl_2/MeOH/NH_4OH = 15/1/0.1 as an eluent. Yield, 57% (4.23 g); yellow oil; R_f = 0.27 (CH_2Cl_2/MeOH/NH_4OH = 9/1/0.5); ^{1}H NMR (400 MHz, $CDCl_3$) δ 0.89 (t, *J* = 7.1 Hz, 3H, CH_3), 1.25-1.35 (m, 4H), 1.42-1.53 (m, 2H), 2.56-2.79 (m, 3H), 2.89 (dd, *J* = 3.5, 12.2 Hz, 1H), 4.71 (dd, *J* = 3.5, 9.4 Hz, 1H), 7.26 (ddd, *J* = 0.6, 4.9, 7.8 Hz, 1H, Ar-H), 7.72 (dtd, *J* = 0.6, 3.9, 7.8 Hz, 1H, Ar-H), 8.49 (dd, *J* = 1.7, 4.9 Hz, 1H, Ar-H), 8.56 (dt, *J* = 0.7, 2.2 Hz, 1H, Ar-H); ^{13}C NMR (100 MHz, $CDCl_3$) δ 13.99, 22.52, 29.35, 29.78, 49.42, 56.88, 69.40, 123.38, 133.60, 138.15, 147.68, 148.74; HRMS (ESI) m/z calculated for $C_{12}H_{21}N_2O$ $[M+H]^+$ 209.1648, found 209.1646.

*2-(Butylamino)-1-(pyridin-3-yl)ethan-1-ol (**12**).* This compound was purified by flash column chromatography using CH_2Cl_2/MeOH/NH_4OH = 15/1/0.1 as an eluent. Yield, 62% (4.29 g); yellow oil; R_f = 0.21 (CH_2Cl_2/MeOH/NH_4OH = 15/1/0.5); ^{1}H NMR (400 MHz, $CDCl_3$) δ 0.89 (t, *J* = 7.2 Hz, 3H, CH_3), 1.27-1.38 (m, 2H), 1.40-1.50 (m, 2H), 2.55-2.72 (m, 5H), 2.85 (dd, *J* = 3.6, 12.3 Hz, 1H), 4.72 (dd, *J* = 3.6, 9.4 Hz, 1H), 7.26 (ddd, *J* = 0.8, 4.9, 7.9 Hz, 1H, Ar-H), 7.71 (app dt, *J* = 2.1, 7.9 Hz, 1H, Ar-H), 8.46 (dd, *J* = 1.6, 4.9 Hz, 1H, Ar-H),

8.54 (d, J = 2.1 Hz, 1H, Ar-H); ^{13}C NMR (100 MHz, $CDCl_3$) δ 13.91, 20.28, 32.14, 40.10, 56.85, 69.36, 123.39, 133.61, 138.14, 147.67, 148.73; HRMS (ESI) m/z calculated for $C_{11}H_{19}N_2O$ $[M+H]^+$ 195.1492, found 195.1492.

2-(Propylamino)-1-(pyridin-3-yl)ethan-1-ol ***(13)***. This compound was purified by flash column chromatography using CH_2Cl_2/MeOH/NH_4OH = 15/1/0.1 as an eluent. Yield, 54% (1.72 g); yellow oil; R_f = 0.26 (CH_2Cl_2/MeOH/NH_4OH = 9/1/0.5); ^{1}H NMR (400 MHz, $CDCl_3$) δ 0.91 (t, J = 7.5 Hz, 3H, CH_3), 1.45-1.55 (m, 2H), 2.54-2.72 (m, 3H), 2.88 (dd, J = 3.6, 12.2 Hz, 1H), 2.98 (br s, 1H), 4.73 (dd, J = 3.4, 9.3 Hz, 1H), 7.26 (dd, J = 4.4, 8.0 Hz, 1H, Ar-H), 7.72 (app dt, J = 1.9, 8.0 Hz, 1H, Ar-H), 8.48 (dd, J = 1.6, 4.8 Hz, 1H, Ar-H), 8.55 (app d, J = 1.9 Hz, 1H, Ar-H); ^{13}C NMR (100 MHz, $CDCl_3$) δ 11.59, 23.09, 51.22, 56.77, 69.37, 123.39, 133.63, 138.15, 147.65, 148.71; HRMS (ESI) m/z calculated for $C_{10}H_{17}N_2O$ $[M+H]^+$ 181.1335, found 181.1335/.

2-(Cyclobutylamino)-1-(pyridin-3-yl)ethan-1-ol ***(14)*** This compound was purified by flash column chromatography using CH_2Cl_2/MeOH/NH_4OH = 15/1/0.1 as an eluent. Yield, 51% (1.73 g); yellow oil; R_f = 0.32 (CH_2Cl_2/MeOH/NH_4OH = 9/1/0.5); ^{1}H NMR (400 MHz, $CDCl_3$) δ 1.55-1.76 (m, 4H), 1.40-1.50 (m, 2H), 2.12-2.26 (m, 2H), 2.59 (dd, J = 9.2, 12.3 Hz, 1H), 2.80 (dd, J = 3.7, 12.3 Hz, 1H), 3.21-3.31 (m, 1H), 4.68 (dd, J = 3.7, 9.2 Hz, 1H), 7.25 (ddd, J = 0.7, 4.9, 8.1 Hz, 1H, Ar-H), 7.70 (dtd, J = 0.5, 4.0, 7.8 Hz, 1H, Ar-H), 8.48 (dd, J = 1.6, 4.9 Hz, 1H, Ar-H), 8.54 (app d, J = 2.2 Hz, 1H, Ar-H); ^{13}C NMR (100 MHz, $CDCl_3$) δ 14.61, 30.85, 30.99, 53.69, 54.09, 69.64, 123.36, 133.56, 138.16, 147.70, 148.77; HRMS (ESI) m/z calculated for $C_{11}H_{17}N_2O$ $[M+H]^+$ 193.1335, found 193.1336.

2-(2-Fluorophenyl)-N-(2-hydroxy-2-(pyridin-3-yl)ethyl)-N-pentylacetamide ***(15)***. This compound was purified by flash column chromatography using CH_2Cl_2/MeOH = 20/1 as an eluent. Yield, 72% (1.04 g); colorless oil; R_f = 0.46 (CH_2Cl_2/MeOH = 9/1); ^{1}H NMR (400 MHz, $CDCl_3$) δ 0.88 (t, J = 7.3 Hz, 3H, CH_3), 1.16-1.34 (m, 4H), 1.43-1.53 (m, 2H), 3.08-3.19 (m, 1H), 3.20-3.30 (m, 1H), 3.52 (dd, J = 2.9, 14.3 Hz, 1H), 3.64-3.79 (m, 3H), 5.01 (dd, J = 2.7, 7.8 Hz, 1H), 5.23 (br s, 1H), 7.02-7.09 (m, 1H, Ar-H), 7.12 (td, J = 1.1, 7.6 Hz, 1H, Ar-H), 7.21-7.34 (m, 3H, Ar-H), 7.72 (dt, J = 1.7, 7.8 Hz, 1H, Ar-H), 8.46 (dd, J = 1.6, 4.9 Hz, 1H, Ar-H), 8.54 (d, J = 1.9 Hz, 1H, Ar-H); ^{13}C NMR (100 MHz, $CDCl_3$) δ 13.84, 22.26, 28.35, 28.70, 32.24 (d, $^3J_{F,C}$ = 2.9 Hz), 50.47, 55.74, 71.72, 115.25 (d, $^2J_{F,C}$ = 22.0 Hz), 121.89 (d, $^2J_{F,C}$ = 15.4 Hz), 123.41, 124.27 (d, $^4J_{F,C}$ = 3.7 Hz), 128.91 (d, $^3J_{F,C}$ = 8.1 Hz),

131.10 (d, $^{3}J_{F,C}$ = 3.7 Hz), 133.75, 137.96, 147.47, 148.76, 160.51 (d, $^{1}J_{F,C}$ = 245.0 Hz), 172.87; HRMS (ESI) m/z calculated for $C_{20}H_{26}N_2O_2F$ $[M+H]^+$ 345.1973, found 345.1965; HPLC purity, 97.40%, t_R = 5.12 min.

N-butyl-2-(2-fluorophenyl)-N-(2-hydroxy-2-(pyridin-3-yl)ethyl)acetamide ***(16)***. This compound was purified by flash column chromatography using CH_2Cl_2/MeOH = 20/1 as an eluent. Yield, 62% (0.72 g); colorless oil; R_f = 0.46 (CH_2Cl_2/MeOH = 9/1); ^{1}H NMR (400 MHz, $CDCl_3$) δ 0.91 (t, J = 7.4 Hz, 3H, CH_3), 1.23-1.35 (m, 2H), 1.43-1.55 (m, 2H), 3.10 (symm m, 1H), 3.27 (symm m, 1H), 3.51 (dd, J = 2.6, 14.4 Hz, 1H), 3.67-3.78 (m, 3H), 5.02 (dd, J = 2.1, 7.9 Hz, 1H), 5.06 (br s, 1H), 7.07 (ddd, J = 1.1, 8.2, 9.6 Hz, 1H, Ar-H), 7.14 (td, J = 1.2, 7.4 Hz, 1H, Ar-H), 7.23-7.26 (m, 1H, Ar-H), 7.26-7.34 (m, 2H, Ar-H), 7.73 (dt, J = 1.9, 7.9 Hz, 1H, Ar-H), 8.50 (dd, J = 1.3, 4.2 Hz, 1H, Ar-H), 8.55 (d, J = 1.2 Hz, 1H, Ar-H); ^{13}C NMR (100 MHz, $CDCl_3$) δ 13.70, 19.87, 30.77, 33.30, 50.34, 55.96, 72.12, 115.34 (d, $^{2}J_{F,C}$ = 21.3 Hz), 121.84 (d, $^{2}J_{F,C}$ = 16.1 Hz), 123.47, 124.35 (d, $^{4}J_{F,C}$ = 3.7 Hz), 129.02 (d, $^{3}J_{F,C}$ = 8.1 Hz), 131.12 (d, $^{3}J_{F,C}$ = 3.7 Hz), 133.71, 137.84, 147.54, 148.93, 160.50 (d, $^{1}J_{F,C}$ = 245.0 Hz), 173.24; HRMS (ESI) m/z calculated for $C_{19}H_{24}N_2O_2F$ $[M+H]^+$ 331.1816, found 331.1808; HPLC purity, 95.28%, t_R = 4.62 min.

2-(2-Fluorophenyl)-N-(2-hydroxy-2-(pyridin-3-yl)ethyl)-N-propylacetamide ***(17)***. This compound was purified by flash column chromatography using CH_2Cl_2/MeOH = 20/1 as an eluent. Yield, 77% (1.21 g); colorless oil; R_f = 0.42 (CH_2Cl_2/MeOH = 9/1); ^{1}H NMR (400 MHz, $CDCl_3$) δ 0.88 (t, J = 7.5 Hz, 3H, CH_3), 1.48-1.61 (m, 2H), 3.09-3.30 (m, 2H), 3.52 (dd, J = 3.1, 14.2 Hz, 1H), 3.66 (dd, J = 7.9, 14.2 Hz, 1H), 3.73 (s, 2H), 5.01 (dd, J = 2.9, 7.9 Hz, 1H), 5.28 (br s, 1H), 7.01-7.09 (m, 1H, Ar-H), 7.12 (td, J = 1.1, 7.5 Hz, 1H, Ar-H), 7.20-7.34 (m, 3H, Ar-H), 7.72 (dt, J = 1.7, 7.8 Hz, 1H, Ar-H), 8.45 (dd, J = 1.7, 4.9 Hz, 1H, Ar-H), 8.53 (d, J = 2.1 Hz, 1H, Ar-H); ^{13}C NMR (100 MHz, $CDCl_3$) δ 10.96, 21.85, 32.24 (d, $^{3}J_{F,C}$ = 2.4 Hz), 51.95, 55.64, 71.57, 115.24 (d, $^{2}J_{F,C}$ = 22.0 Hz), 121.89 (d, $^{2}J_{F,C}$ = 16.1 Hz), 123.40, 124.24 (d, $^{4}J_{F,C}$ = 3.7 Hz), 128.89 (d, $^{3}J_{F,C}$ = 8.1 Hz), 131.11 (d, $^{3}J_{F,C}$ = 3.7 Hz), 133.77, 137.99, 147.41, 148.69, 160.50 (d, $^{1}J_{F,C}$ = 245.8 Hz), 172.78; HRMS (ESI) m/z calculated for $C_{18}H_{22}N_2O_2F$ $[M+H]^+$ 317.1660, found 317.1653; HPLC purity, 98.13%, t_R = 4.13 min.

N-cyclobutyl-2-(2-fluorophenyl)-N-(2-hydroxy-2-(pyridin-3-yl)ethyl)acetamide ***(18)***. This compound was purified by flash column chromatography using CH_2Cl_2/MeOH = 15/1 as an eluent. Yield, 66% (1.04 g); colorless oil; R_f = 0.52 (CH_2Cl_2/MeOH = 9/1); ^{1}H NMR (400

MHz, $CDCl_3$) δ 1.48-1.70 (m, 2H), 1.85-2.16 (m, 4H), 3.48 (dd, *J* = 2.8, 14.6 Hz, 1H), 3.75 (s, 2H), 3.75-3.82 (m, 1H), 4.26 (symm m, 1H), 4.90 (dd, *J* = 2.0, 8.3 Hz, 1H), 5.37 (br s, 1H), 7.01-7.13 (m, 2H, Ar-H), 7.16-7.30 (m, 3H, Ar-H), 7.74 (dt, *J* = 1.6, 7.8 Hz, 1H, Ar-H), 8.47 (dd, *J* = 1.2, 4.6 Hz, 1H, Ar-H), 8.55 (d, *J* = 1.8 Hz, 1H, Ar-H); ^{13}C NMR (100 MHz, $CDCl_3$) δ 14.42, 28.97, 29.56, 33.99 (d, $^3J_{F,C}$ = 2.2 Hz), 50.97, 52.42, 72.56, 115.24 (d, $^2J_{F,C}$ = 21.3 Hz), 121.79 (d, $^2J_{F,C}$ = 16.1 Hz), 123.44, 124.22 (d, $^4J_{F,C}$ = 3.7 Hz), 128.90 (d, $^3J_{F,C}$ = 8.1 Hz), 130.97 (d, $^3J_{F,C}$ = 3.7 Hz), 133.77, 138.15, 147.54, 148.86, 160.52 (d, $^1J_{F,C}$ = 245.8 Hz), 173.34; HRMS (ESI) m/z calculated for $C_{19}H_{22}N_2O_2F$ $[M+H]^+$ 329.1660, found 329.1654; HPLC purity, 96.67%, t_R = 4.30 min.

2-(2-Chlorophenyl)-N-(2-hydroxy-2-(pyridin-3-yl)ethyl)-N-pentylacetamide ***(19)***. This compound was purified by flash column chromatography using CH_2Cl_2/MeOH = 20/1 as an eluent. Yield, 74% (0.99 g); colorless oil; R_f = 0.48 (CH_2Cl_2/MeOH = 9/1); ^{1}H NMR (400 MHz, $CDCl_3$) δ 0.89 (t, *J* = 7.3 Hz, 3H, CH_3), 1.19-1.36 (m, 4H), 1.48-1.60 (m, 2H), 3.12 (symm m, 1H), 3.22-3.32 (m, 1H), 3.53 (dd, *J* = 2.7, 14.3 Hz, 1H), 3.74 (dd, *J* = 8.1, 14.3 Hz, 1H), 3.81 (d, A of AB, J_{AB} = 15.9 Hz, 1H), 3.85 (d, B of AB, J_{AB} = 15.9 Hz, 1H), 5.03 (d, *J* = 7.1 Hz, 1H), 5.10 (br s, 1H), 7.22-7.29 (m, 3H, Ar-H), 7.30-7.34 (m, 1H, Ar-H), 7.37-7.42 (m, 1H, Ar-H), 7.76 (dtd, *J* = 0.5, 3.9, 7.8 Hz, 1H, Ar-H), 8.51 (dd, *J* = 1.7, 4.9 Hz, 1H, Ar-H), 8.57 (app d, *J* = 2.2 Hz, 1H, Ar-H); ^{13}C NMR (100 MHz, $CDCl_3$) δ 13.88, 22.32, 28.36, 28.78, 38.02, 50.57, 55.92, 72.05, 123.46, 127.08, 128.64, 129.47, 131.05, 132.95, 133.75, 134.01, 137.89, 147.58, 148.91, 173.09; HRMS (ESI) m/z calculated for $C_{20}H_{26}N_2O_2Cl$ $[M+H]^+$ 361.1677, found 361.1670; HPLC purity, 95.41%, t_R = 5.43 min.

N-butyl-2-(2-chlorophenyl)-N-(2-hydroxy-2-(pyridin-3-yl)ethyl)acetamide ***(20)***. This compound was purified by flash column chromatography using CH_2Cl_2/MeOH = 15/1 as an eluent. Yield, 71% (0.98 g); colorless oil; R_f = 0.36 (CH_2Cl_2/MeOH = 9/1); ^{1}H NMR (400 MHz, $CDCl_3$) δ 0.92 (t, *J* = 7.4 Hz, 3H, CH_3), 1.22-1.36 (m, 2H), 1.46-1.60 (m, 2H), 3.08-3.18 (m, 1H), 3.22-3.32 (m, 1H), 3.52 (dd, *J* = 2.5, 14.4 Hz, 1H), 3.74 (dd, *J* = 7.9, 14.4 Hz, 1H), 3.82 (d, A of AB, J_{AB} = 15.9 Hz, 1H), 3.86 (d, B of AB, J_{AB} = 15.9 Hz, 1H), 5.03 (d, *J* = 8.3 Hz, 1H), 5.07 (br s, 1H), 7.17-7.35 (m, 4H, Ar-H), 7.38-7.42 (m, 1H, Ar-H), 7.77 (dt, *J* = 1.9, 7.9 Hz, 1H, Ar-H), 8.50 (dd, *J* = 1.6, 4.8 Hz, 1H, Ar-H), 8.57 (d, *J* = 1.8 Hz, 1H, Ar-H); ^{13}C NMR (100 MHz, $CDCl_3$) δ 13.71, 19.90, 30.74, 38.00, 50.32, 55.85, 71.94, 123.46, 127.07, 128.62, 129.45, 131.03, 132.94, 133.77, 134.01, 137.91, 147.53, 148.86, 173.02;

HRMS (ESI) m/z calculated for $C_{19}H_{24}N_2O_2Cl$ $[M+H]^+$ 347.1521, found 347.1515; HPLC purity, 97.83%, t_R = 4.97 min.

*N-(2-hydroxy-2-(pyridin-3-yl)ethyl)-N-pentyl-2-phenylacetamide (**21**).* This compound was purified by flash column chromatography using CH_2Cl_2/MeOH = 20/1 as an eluent. Yield, 75% (0.95 g); colorless oil; R_f = 0.58 (CH_2Cl_2/MeOH = 9/1); ^{1}H NMR (400 MHz, $CDCl_3$) δ 0.87 (t, *J* = 7.3 Hz, 3H, CH_3), 1.12-1.34 (m, 4H), 1.36-1.50 (m, 2H), 3.01 (symm m, 1H), 3.26 (symm m, 1H), 3.49 (dd, *J* = 2.4, 14.3 Hz, 1H), 3.70-3.80 (m, 3H), 5.00 (dt, *J* = 2.6, 7.7 Hz, 1H), 5.20 (d, *J* = 3.8 Hz, 1H), 7.19-7.26 (m, 2H, Ar-H), 7.27-7.30 (m, 2H, Ar-H), 7.32-7.38 (m, 2H, Ar-H), 7.70 (dtd, *J* = 0.6, 3.9, 7.8 Hz, 1H, Ar-H), 8.49 (dd, *J* = 1.7, 4.8 Hz, 1H, Ar-H), 8.55 (app d, *J* = 2.2 Hz, 1H, Ar-H); ^{13}C NMR (100 MHz, $CDCl_3$) δ 13.89, 22.32, 28.42, 28.78, 40.70, 50.63, 55.89, 72.38, 123.44, 127.11, 128.76, 128.81, 133.69, 134.47, 137.81, 147.61, 148.99, 174.35; HRMS (ESI) m/z calculated for $C_{20}H_{27}N_2O_2$ $[M+H]^+$ 327.2067, found 327.2059; HPLC purity, 97.35%, t_R = 5.01 min.

*N-butyl-N-(2-hydroxy-2-(pyridin-3-yl)ethyl)-2-phenylacetamide (**22**).* This compound was purified by flash column chromatography using CH_2Cl_2/MeOH = 15/1 as an eluent. Yield, 70% (0.77 g); colorless oil; R_f = 0.48 (CH_2Cl_2/MeOH = 9/1); ^{1}H NMR (400 MHz, $CDCl_3$) δ 0.88 (t, *J* = 7.4 Hz, 3H, CH_3), 1.18-1.30 (m, 2H), 1.36-1.50 (m, 2H), 3.04 (symm m, 1H), 3.23 (symm m, 1H), 3.49 (dd, *J* = 2.6, 14.2 Hz, 1H), 3.68-3.82 (m, 3H), 4.98-5.04 (m, 1H), 5.26 (d, *J* = 3.8 Hz, 1H), 7.18-7.32 (m, 4H, Ar-H), 7.32-7.40 (m, 2H, Ar-H), 7.71 (app dt, *J* = 2.2, 7.9 Hz, 1H, Ar-H), 8.49 (dd, *J* = 1.5, 4.8 Hz, 1H, Ar-H), 8.54 (d, *J* = 2.1 Hz, 1H, Ar-H); ^{13}C NMR (100 MHz, $CDCl_3$) δ 13.70, 19.88, 30.75, 40.66, 50.35, 55.81, 72.23, 123.44, 127.08, 128.75, 128.79, 133.72, 134.45, 137.83, 147.55, 148.92, 174.25; HRMS (ESI) m/z calculated for $C_{19}H_{25}N_2O_2$ $[M+H]^+$ 313.1911, found 313.1903; HPLC purity, 98.01%, t_R = 4.52 min.

*N-butyl-2-(3,4-difluorophenyl)-N-(2-hydroxy-2-(pyridin-3-yl)ethyl)acetamide (**23**).* This compound was purified by flash column chromatography using CH_2Cl_2/MeOH = 15/1 as an eluent. Yield, 67% (0.93 g); colorless oil; R_f = 0.43 (CH_2Cl_2/MeOH = 9/1); ^{1}H NMR (400 MHz, $CDCl_3$) δ 0.92 (t, *J* = 7.3 Hz, 3H, CH_3), 1.23-1.36 (m, 2H), 1.44-1.58 (m, 2H), 3.06-3.18 (m, 1H), 3.20-3.32 (m, 1H), 3.50 (dd, *J* = 2.5, 14.3 Hz, 1H), 3.62-3.78 (m, 3H), 4.90 (br s, 1H), 5.02 (d, *J* = 7.1 Hz, 1H), 6.93-6.98 (m, 1H, Ar-H), 7.04-7.18 (m, 2H, Ar-H), 7.24-7.30 (m, 1H, Ar-H), 7.73 (app dt, *J* = 1.9, 7.9 Hz, 1H, Ar-H), 8.51 (dd, *J* = 1.5, 4.8 Hz, 1H, Ar-H), 8.56 (d, *J* = 1.8 Hz, 1H, Ar-H); ^{13}C NMR (100 MHz, $CDCl_3$) δ 13.72, 19.92, 30.88, 39.31,

50.30, 55.70, 71.98, 117.39 (d, $^{2}J_{F,C}$ = 17.6 Hz), 118.04 (d, $^{2}J_{F,C}$ = 17.6 Hz), 123.49, 125.01 (dd, $^{3}J_{F,C}$ = 6.6 Hz, $^{4}J_{F,C}$ = 3.7 Hz), 131.35 (dd, $^{3}J_{F,C}$ = 5.9 Hz, $^{4}J_{F,C}$ = 4.4 Hz), 133.68, 137.74, 147.50, 149.90, 149.52 (dd, $^{1}J_{F,C}$ = 248.0 Hz, $^{2}J_{F,C}$ = 12.5 Hz), 150.35 (dd, $^{1}J_{F,C}$ = 248.7 Hz, $^{2}J_{F,C}$ = 13.2 Hz), 173.09; HRMS (ESI) m/z calculated for $C_{19}H_{23}N_2O_2F_2$ $[M+H]^+$ 349.1722, found 349.1715; HPLC purity, 93.80%, t_R = 4.83 min.

N-butyl-2-cyclohexyl-N-(2-hydroxy-2-(pyridin-3-yl)ethyl)acetamide ***(33)***. This compound was purified by flash column chromatography using CH_2Cl_2/MeOH = 15/1 as an eluent. Yield, 69% (0.93 g); colorless oil; R_f = 0.41 (CH_2Cl_2/MeOH = 9/1); ^{1}H NMR (400 MHz, $CDCl_3$) δ 0.80-0.98 (m, 5H, CH_3 and cyclohexyl-H), 1.03-1.16 (m, 1H), 1.17-1.32 (m, 4H), 1.36-1.50 (m, 2H), 1.56-1.94 (m, 4H, overlapping with H_2O), 2.01-2.04 (m, 2H), 2.16 (app d, *J* = 6.7 Hz, 2H), 2.99-3.10 (m, 1H), 3.10-3.22 (m, 1H), 3.43 (dd, *J* = 2.9, 14.3 Hz, 1H), 3.60-3.72 (m, 1H), 4.97 (dd, *J* = 2.2, 7.8 Hz, 1H), 7.08 (br s, 1H), 7.26-7.32 (m, 1H, Ar-H), 7.79 (app dd, *J* = 1.1, 7.9 Hz, 1H, Ar-H), 8.42-8.47 (m, 1H, Ar-H), 8.50-8.54 (m, 1H, Ar-H); ^{13}C NMR (100 MHz, $CDCl_3$) δ 13.65, 19.79, 26.02, 26.08, 30.86, 33.23, 35.01, 40.46, 50.04, 55.43, 71.78, 123.63, 134.42, 138.45, 146.66, 147.85, 175.54; HRMS (ESI) m/z calculated for $C_{19}H_{31}N_2O_2$ $[M+H]^+$ 319.2380, found 319.2375; HPLC purity, 97.08%, t_R = 5.35 min.

2-((2-Fluorophenethyl)(pentyl)amino)-1-(pyridin-3-yl)ethan-1-ol ***(24)***. This compound was purified by flash column chromatography using CH_2Cl_2/MeOH = 20/1 as an eluent. Yield, 61% (0.56 g); colorless oil; R_f = 0.49 (CH_2Cl_2/MeOH/NH_4OH = 15/1/0.1); ^{1}H NMR (400 MHz, $CDCl_3$) δ 0.90 (t, J = 7.2 Hz, 3H, CH_3), 1.20-1.38 (m, 4H), 1.40-1.58 (m, 2H), 2.48 (dd, *J* = 10.6, 12.2 Hz, 1H), 2.50-2.60 (m, 1H), 2.64-2.83 (m, 4H), 2.84-2.95 (m, 2H), 3.95 (br s, 1H), 4.61 (dd, *J* = 3.4, 10.5 Hz, 1H), 7.00-7.11 (m, 2H, Ar-H), 7.17-7.24 (m, 2H, Ar-H), 7.27 (ddd, J = 0.5, 4.8, 7.7 Hz, 1H, Ar-H), 7.71 (dt, *J* = 1.7, 7.9 Hz, 1H, Ar-H), 8.52 (dd, *J* = 1.7, 4.9 Hz, 1H, Ar-H), 8.56 (d, *J* = 2.2 Hz, 1H, Ar-H); ^{13}C NMR (100 MHz, $CDCl_3$) δ 14.02, 22.56, 26.77, 27.08 (d, $^{3}J_{F,C}$ = 2.2 Hz), 29.46, 53.71, 53.88, 62.63, 67.38, 115.32 (d, $^{2}J_{F,C}$ = 22.7 Hz), 123.34, 124.06 (d, $^{4}J_{F,C}$ = 2.9 Hz), 126.77 (d, $^{2}J_{F,C}$ = 16.1 Hz), 128.03 (d, $^{3}J_{F,C}$ = 8.1 Hz), 130.96 (d, $^{3}J_{F,C}$ = 5.1 Hz), 133.53, 137.67, 147.80, 148.83, 161.09 (d, $^{1}J_{F,C}$ = 245.0 Hz); HRMS (ESI) m/z calculated for $C_{20}H_{28}N_2OF$ $[M+H]^+$ 331.2180, found 331.2172; HPLC purity, 96.89%, t_R = 4.16 min; ^{1}H NMR of dihydrobromide salt (400 MHz, DMSO-d_6) δ 0.90 (q, *J* = 7.2 Hz, 3H), 1.25-1.41 (m, 4H), 1.63-1.82 (m, 2H), 2.91-3.50 (m, 8H, overlapping with water in DMSO), 5.34 (dd, *J* = 3.7, 9.4 Hz, 1H), 6.68 (br s, 1H) 7.17-7.28 (m, 2H, Ar-H),

7.31-7.50 (m, 2H, Ar-H), 7.92 (app t, *J* = 7.0 Hz, 1H, Ar-H), 8.42 (app d, *J* = 7.0 Hz, 1H, Ar-H), 8.82 (d, *J* = 5.1 Hz, 1H, Ar-H), 8.91 (dd, *J* = 1.3, 7.4 Hz, 1H, Ar-H), 9.59 (br s, 1H).

*2-(Butyl(2-fluorophenethyl)amino)-1-(pyridin-3-yl)ethan-1-ol (**25**).* This compound was purified by two consecutive flash column chromatographies using CH_2Cl_2/MeOH/NH_4OH = 20/1/0.1 and EtOAc/MeOH = 40/1 as eluents. Yield, 51% (0.23 g); colorless oil; R_f = 0.50 (EtOAc/MeOH = 9/1); ^{1}H NMR (400 MHz, $CDCl_3$) δ 0.93 (t, *J* = 7.3 Hz, 3H, CH_3), 1.26-1.38 (m, 2H), 1.40-1.55 (m, 2H), 2.48 (dd, *J* = 10.6, 13.1 Hz, 1H), 2.52-2.60 (m, 1H), 2.65-2.75 (m, 2H), 2.76-2.82 (m, 2H), 2.84-2.94 (m, 2H), 3.93 (br s, 1H), 4.61 (dd, *J* = 3.4, 10.6 Hz, 1H), 7.00-7.11 (m, 2H, Ar-H), 7.17-7.24 (m, 2H, Ar-H), 7.27 (ddd, *J* = 0.9, 4.9, 7.9 Hz, 1H, Ar-H), 7.71 (dtd, *J* = 0.6, 1.8, 7.9 Hz, 1H, Ar-H), 8.51 (dd, *J* = 1.7, 4.9 Hz, 1H, Ar-H), 8.56 (dt, *J* = 0.6, 2.2 Hz, 1H, Ar-H); ^{13}C NMR (100 MHz, $CDCl_3$) δ 13.99, 20.42, 26.95, 29.09, 53.45, 53.85, 62.57, 67.29, 115.34 (d, $^2J_{F,C}$ = 22.0 Hz), 123.37, 124.08 (d, $^4J_{F,C}$ = 2.9 Hz), 126.60 (d, $^2J_{F,C}$ = 16.1 Hz), 128.08 (d, $^3J_{F,C}$ = 8.1 Hz), 130.96 (d, $^3J_{F,C}$ = 4.4 Hz), 133.56, 137.60, 147.74, 148.82, 161.08 (d, $^1J_{F,C}$ = 245.0 Hz); HRMS (ESI) m/z calculated for $C_{19}H_{26}N_2OF$ $[M+H]^+$ 317.2024, found 317.2018; HPLC purity, 96.22%, tR = 3.65 min; ^{1}H NMR of dihydrobromide salt (400 MHz, DMSO-d_6) δ 0.94 (dt, J = 7.3, 14.7 Hz, 3H), 1.35 (symm m, 2H), 1.60-1.82 (m, 2H), 3.04-3.55 (m, 8H, overlapping with water in DMSO), 5.36 (dd, *J* = 3.1, 9.5 Hz, 1H), 6.67 (br s 1H) 7.16-7.28 (m, 2H, Ar-H), 7.30-7.51 (m, 2H, Ar-H), 7.94 (app t, *J* = 6.5 Hz, 1H, Ar-H), 8.45 (app t, *J* = 6.5 Hz, 1H, Ar-H), 8.83 (d, *J* = 5.2 Hz, 1H, Ar-H), 8.92 (dd, *J* = 1.2, 8.1 Hz, 1H, Ar-H), 9.61 (br s, 1H).

*2-((2-Fluorophenethyl)(propyl)amino)-1-(pyridin-3-yl)ethan-1-ol (**26**)*. This compound was purified by two consecutive flash column chromatographies using CH_2Cl_2/MeOH/NH_4OH = 20/1/0.1 and EtOAc/MeOH = 50/1 as eluents. Yield, 54% (0.56 g); colorless oil; R_f = 0.33 (CH_2Cl_2/MeOH/NH_4OH = 15/1/0.1); ^{1}H NMR (400 MHz, $CDCl_3$) δ 0.90 (t, *J* = 7.3 Hz, 3H, CH_3), 1.42-1.62 (m, 2H), 2.49 (dd, *J* = 10.6, 13.1 Hz, 1H), 2.50-2.57 (m, 1H), 2.60-2.71 (m, 2H), 2.73-2.83 (m, 2H), 2.84-2.95 (m, 2H), 3.94 (br s, 1H), 4.61 (dd, *J* = 3.4, 10.6 Hz, 1H), 7.00-7.11 (m, 2H, Ar-H), 7.17-7.23 (m, 2H, Ar-H), 7.27 (ddd, *J* = 0.6, 4.8, 7.8 Hz, 1H, Ar-H), 7.71 (dtd, *J* = 0.6, 2.3, 7.8 Hz, 1H, Ar-H), 8.51 (dd, *J* = 1.8, 4.9 Hz, 1H, Ar-H), 8.56 (dt, *J* = 0.7, 2.3 Hz, 1H, Ar-H); ^{13}C NMR (100 MHz, $CDCl_3$) δ 11.68, 20.27, 27.03 (d, $^3J_{F,C}$ = 2.2 Hz), 53.93, 55.67, 62.64, 67.37, 115.36 (d, $^2J_{F,C}$ = 22.0 Hz), 123.37, 124.10 (d, $^4J_{F,C}$ = 3.7 Hz), 126.69 (d, $^2J_{F,C}$ = 16.1 Hz), 128.08 (d, $^3J_{F,C}$ = 8.1 Hz), 130.97 (d, $^3J_{F,C}$ = 5.1 Hz), 133.55, 137.63, 147.81, 148.87, 161.08 (d, $^1J_{F,C}$ = 245.0 Hz); HRMS (ESI) m/z calculated for

$C_{18}H_{24}N_2OF$ $[M+H]^+$ 303.1867, found 303.1861; HPLC purity, 97.73%, t_R = 3.19 min; ^1H NMR of dihydrobromide salt (400 MHz, DMSO-d_6) δ 0.90 (p, *J* = 7.1 Hz, 3H), 1.25-1.41 (m, 4H), 1.66-1.90 (m, 2H), 3.02-3.60 (m, 8H, overlapping with water in DMSO), 5.43 (dd, *J* = 2.4, 10.2 Hz, 1H), 6.73 (br s 1H) 7.16-7.27 (m, 2H, Ar-H), 7.30-7.52 (m, 2H, Ar-H), 8.05 (app t, *J* = 6.4 Hz, 1H, Ar-H), 8.60 (app t, *J* = 6.4 Hz, 1H, Ar-H), 8.89 (d, *J* = 5.1 Hz, 1H, Ar-H), 9.01 (app d, *J* = 6.4 Hz, 1H, Ar-H), 9.68 (br s, 1H).

*2-(Cyclobutyl(2-fluorophenethyl)amino)-1-(pyridin-3-yl)ethan-1-ol (**27**).* This compound was purified by flash column chromatography using CH_2Cl_2/MeOH = 20/1 as an eluent. Yield, 69% (0.66 g); colorless oil; R_f = 0.49 (CH_2Cl_2/MeOH/NH_4OH = 15/1/0.1); ^1H NMR (400 MHz, $CDCl_3$) *δ* 1.56-1.70 (m, 2H), 1.80 (p, *J* = 9.9 Hz, 1H), 1.84-1.97 (m, 1H), 1.97-2.14 (m, 2H), 2.47 (dd, *J* = 10.5, 13.0 Hz, 1H), 2.60 (dd, *J* = 3.8, 13.0 Hz, 1H), 2.68-2.90 (m, 4H), 3.30 (symm m, 1H), 4.16 (br s, 1H), 4.60 (dd, *J* = 3.5, 10.4 Hz, 1H), 5.37 (br s, 1H), 6.97-7.07 (m, 2H, Ar-H), 7.12-7.20 (m, 2H, Ar-H), 7.23 (ddd, *J* = 0.6, 4.9, 7.8 Hz, 1H, Ar-H), 7.71 (dt, *J* = 1.7, 7.8 Hz, 1H, Ar-H), 8.46 (dd, *J* = 1.7, 4.9 Hz, 1H, Ar-H), 8.53 (app d, *J* = 2.1 Hz, 1H, Ar-H); ^{13}C NMR (100 MHz, $CDCl_3$) *δ* 14.20, 26.47, 28.00, 28.67, 51.20, 57.64, 58.61, 67.42, 115.19 (d, $^2J_{F,C}$ = 22.0 Hz), 123.25, 123.97 (d, $^4J_{F,C}$ = 3.7 Hz), 126.70 (d, $^2J_{F,C}$ = 15.4 Hz), 127.87 (d, $^3J_{F,C}$ = 8.8 Hz), 130.80 (d, $^3J_{F,C}$ = 5.1 Hz), 133.48, 137.87, 147.60, 148.59, 161.00 (d, $^1J_{F,C}$ = 245.0 Hz); HRMS (ESI) m/z calculated for $C_{19}H_{24}N_2OF$ $[M+H]^+$ 315.1867, found 315.1861; HPLC purity, 97.30%, t_R = 3.25 min; ^1H NMR of dihydrobromide salt (400 MHz, DMSO-d_6) *δ* 1.60-1.84 (m, 2H), 2.16-2.35 (m, 2H), 2.36-2.58 (m, 2H, overlapping with water in DMSO), 3.02-3.54 (m, 6H), 3.95-4.20 (m, 1H), 5.30-5.46 (m, 1H), 6.74 (br s, 1H), 7.16-7.28 (m, 2H, Ar-H), 7.30-7.58 (m, 2H, Ar-H), 8.06 (dd, *J* = 5.7, 7.9 Hz, 1H, Ar-H), 8.64 (app d, *J* = 8.1 Hz, 1H, Ar-H), 8.91 (d, *J* = 5.2 Hz, 1H, Ar-H), 9.04 (d, *J* = 1.6Hz, 1H, Ar-H), 9.85 and 10.02 (br s, 1H).

*2-((2-Chlorophenethyl)(pentyl)amino)-1-(pyridin-3-yl)ethan-1-ol (**28**).* This compound was purified by flash column chromatography using CH_2Cl_2/MeOH = 20/1 as an eluent. Yield, 65% (0.42 g); colorless oil; R_f = 0.41 (CH_2Cl_2/MeOH = 9/1); ^1H NMR (400 MHz, $CDCl_3$) *δ* 0.91 (t, *J* = 7.2 Hz, 3H, CH_3), 1.22-1.40 (m, 4H), 1.42-1.58 (m, 2H), 2.50 (dd, *J* = 10.8, 13.0 Hz, 1H), 2.53-2.61 (m, 1H), 2.65-3.02 (m, 6H), 4.00 (br s, 1H), 4.63 (dd, *J* = 3.4, 10.5 Hz, 1H), 7.14-7.24 (m, 3H, Ar-H), 7.27 (ddd, *J* = 0.7, 4.9, 7.8 Hz, 1H, Ar-H), 7.34-7.38 (m, 1H, Ar-H), 7.72 (dtd, *J* = 0.7, 2.2, 7.9 Hz, 1H, Ar-H), 8.52 (dd, *J* = 1.7, 4.9 Hz, 1H, Ar-H), 8.57 (dt, *J* = 0.7, 2.2 Hz, 1H, Ar-H); ^{13}C NMR (100 MHz, $CDCl_3$) *δ* 14.02, 22.54, 26.42, 29.41,

30.96, 53.40, 53.88, 62.52, 67.29, 123.44, 126.99, 127.99, 129.68, 130.99, 133.64, 133.89, 137.00, 137.49, 147.70, 148.87; HRMS (ESI) m/z calculated for $C_{20}H_{28}N_2OCl$ $[M+H]^+$ 347.1885, found 347.1878; HPLC purity, 97.94%, t_R = 4.47 min.

2-(Butyl(2-chlorophenethyl)amino)-1-(pyridin-3-yl)ethan-1-ol ***(29)***. This compound was purified by flash column chromatography using CH_2Cl_2/MeOH/NH_4OH = 15/1/0.1 as an eluent. Yield, 59% (0.38 g); colorless oil; R_f = 0.48 (CH_2Cl_2/MeOH/NH_4OH = 15/1/0.1); ^1H NMR (400 MHz, $CDCl_3$) δ 0.94 (t, J = 7.4 Hz, 3H, CH_3), 1.28-1.40 (m, 2H), 1.44-1.54 (m, 2H), 2.50 (dd, J = 10.6, 12.8 Hz, 1H), 2.57 (symm m, 1H), 2.68-3.02 (m, 6H), 4.00 (br s, 1H), 4.63 (dd, J = 3.5, 10.5 Hz, 1H), 7.14-7.24 (m, 3H, Ar-H), 7.26-7.30 (m, 1H, Ar-H), 7.34-7.38 (m, 1H, Ar-H), 7.72 (app dt, J = 1.8, 7.8 Hz, 1H, Ar-H), 8.52 (dd, J = 1.8, 4.9 Hz, 1H, Ar-H), 8.57 (dt, J = 0.5, 2.3 Hz, 1H, Ar-H); ^{13}C NMR (100 MHz, $CDCl_3$) δ 14.02, 20.45, 29.35, 31.25, 53.34, 53.45, 62.52, 67.40, 123.35, 126.87, 127.81, 129.63, 130.90, 133.52, 133.88, 137.42, 137.64, 147.81, 148.85; HRMS (ESI) m/z calculated for $C_{19}H_{26}N_2OCl$ $[M+H]^+$ 333.1728, found 333.1725; HPLC purity, 95.41%, t_R = 4.03 min.

2-(Pentyl(phenethyl)amino)-1-(pyridin-3-yl)ethan-1-ol ***(30)***. This compound was purified by flash column chromatography using CH_2Cl_2/MeOH = 20/1 as an eluent. Yield, 48% (0.40 g); colorless oil; R_f = 0.38 (CH_2Cl_2/MeOH = 9/1); ^1H NMR (400 MHz, $CDCl_3$) δ 0.91 (t, J = 7.2 Hz, 3H, CH_3), 1.23-1.38 (m, 4H), 1.40-1.55 (m, 2H), 2.40 (dd, J = 10.5, 12.8 Hz, 1H), 2.55 (symm m, 1H), 2.66-2.92 (m, 6H), 3.99 (br s, 1H), 4.59 (dd, J = 3.5, 10.6 Hz, 1H), 7.17-7.25 (m, 3H, Ar-H), 7.29-7.35 (m, 2H, Ar-H), 7.46 (app dd, J = 5.6, 7.9 Hz, 1H, Ar-H), 7.91 (app dt, J = 1.3, 7.9 Hz, 1H, Ar-H), 8.49 (app d, J = 5.3 Hz, 1H, Ar-H), 8.55 (app d, J = 1.7 Hz, 1H, Ar-H); ^{13}C NMR (100 MHz, $CDCl_3$) δ 14.01, 22.53, 26.59, 29.42, 33.59, 53.68, 55.37, 62.62, 67.32, 123.34, 126.21, 128.53, 128.62, 133.54, 137.69, 139.86, 147.72, 148.79; HRMS (ESI) m/z calculated for $C_{20}H_{29}N_2O$ $[M+H]^+$ 313.2274, found 313.2267; HPLC purity, 96.02%, t_R = 4.12 min.

2-(Butyl(phenethyl)amino)-1-(pyridin-3-yl)ethan-1-ol ***(31)***. This compound was purified by two consecutive flash column chromatographies using CH_2Cl_2/MeOH/NH_4OH = 30/1/0.1 and EtOAc/MeOH = 30/1 as eluents. Yield, 58% (0.38 g); colorless oil; R_f = 0.50 (CH_2Cl_2/MeOH/NH_4OH = 15/1/0.1); ^1H NMR (400 MHz, $CDCl_3$) δ 0.93 (t, J = 7.4 Hz, 3H, CH_3), 1.24-1.38 (m, 2H), 1.40-1.56 (m, 2H), 2.48 (dd, J = 10.6, 12.8 Hz, 1H), 2.50-2.59 (m, 1H), 2.64-2.95 (m, 6H), 3.97 (br s, 1H), 4.60 (dd, J = 3.4, 10.5 Hz, 1H), 7.18-7.25 (m, 3H, Ar-

H), 7.25-7.35 (m, 3H, Ar-H), 7.70 (dtd, *J* = 0.7, 2.2, 7.9 Hz, 1H, Ar-H), 8.52 (dd, *J* = 1.7, 4.8 Hz, 1H, Ar-H), 8.55 (app d, *J* = 2.2 Hz, 1H, Ar-H); ^{13}C NMR (100 MHz, $CDCl_3$) δ 14.04, 20.49, 29.22, 33.69, 53.49, 55.53, 62.67, 67.35, 123.34, 126.22, 128.49, 128.66, 133.49, 137.69, 139.96, 147.83, 148.87; HRMS (ESI) m/z calculated for $C_{19}H_{27}N_2O$ $[M+H]^+$ 299.2118, found 299.2113; HPLC purity, 99.05%, t_R = 3.55 min.

2-(Butyl(3,4-difluorophenethyl)amino)-1-(pyridin-3-yl)ethan-1-ol (***32***). This compound was purified by two consecutive flash column chromatographies using CH_2Cl_2/MeOH/NH_4OH = 20/1/0.1 and EtOAc/MeOH = 40/1 as eluents. Yield, 64% (0.22 g); colorless oil; R_f = 0.48 (CH_2Cl_2/MeOH/NH_4OH = 15/1/0.1); ^{1}H NMR (400 MHz, $CDCl_3$) δ 0.92 (t, *J* = 7.4 Hz, 3H, CH_3), 1.25-1.35 (m, 2H), 1.38-1.52 (m, 2H), 2.48 (dd, *J* = 10.3, 12.7 Hz, 1H), 2.48-2.56 (m, 1H), 2.64-2.90 (m, 6H), 4.61 (dd, *J* = 3.6, 10.4 Hz, 1H), 6.86-6.92 (m, 1H, Ar-H), 6.98-7.11 (m, 2H, Ar-H), 7.26 (ddd, *J* = 0.6, 4.9, 7.9 Hz, 1H, Ar-H), 7.70 (dtd, *J* = 0.5, 2.1, 7.8 Hz, 1H, Ar-H), 8.50 (dd, *J* = 1.6, 4.8 Hz, 1H, Ar-H), 8.55 (app d, *J* = 2.0 Hz, 1H, Ar-H); ^{13}C NMR (100 MHz, $CDCl_3$) δ 13.98, 20.45, 28.86, 32.71, 53.59, 55.35, 62.56, 67.25, 117.23 (d, $^2J_{F,C}$ = 17.6 Hz), 117.34 (d, $^2J_{F,C}$ = 16.9 Hz), 123.49, 124.50 (dd, $^3J_{F,C}$ = 6.6 Hz, $^4J_{F,C}$ = 3.7 Hz), 133.64, 136.51 (dd, $^3J_{F,C}$ = 5.9 Hz, $^4J_{F,C}$ = 5.0 Hz), 137.51, 147.58, 148.83, 148.94 (dd, $^1J_{F,C}$ = 245.8 Hz, $^2J_{F,C}$ = 13.2 Hz), 150.22 (dd, $^1J_{F,C}$ = 248.0 Hz, $^2J_{F,C}$ = 13.2 Hz); HRMS (ESI) m/z calculated for $C_{19}H_{25}N_2OF_2$ $[M+H]^+$ 335.1930, found 335.1921; HPLC purity, 95.08%, t_R = 3.94 min.

2-(Butyl(2-cyclohexylethyl)amino)-1-(pyridin-3-yl)ethan-1-ol (***34***). This compound was purified by two consecutive flash column chromatographies using CH_2Cl_2/MeOH/NH_4OH = 20/1/0.1 and EtOAc/MeOH = 30/1 as eluents. Yield, 59% (0.28 g); colorless oil; R_f = 0.64 (CH_2Cl_2/MeOH/NH_4OH = 15/1/0.1); ^{1}H NMR (400 MHz, $CDCl_3$) δ 0.84-0.98 (m, 6H, CH_3 and cyclohexyl-H), 1.14-1.40 (m, 8H), 1.42-1.50 (m, 2H), 1.64-1.75 (m, 4H, overlapping with H_2O), 2.39-2.51 (m, 3H), 2.57-2.71 (m, 3H), 4.32 (br s, 1H), 4.65 (dd, *J* = 3.5, 10.5 Hz, 1H), 7.27 (ddd, *J* = 0.6, 4.9, 7.8 Hz, 1H, Ar-H), 7.73 (dtd, *J* = 0.6, 2.3, 7.9 Hz, 1H, Ar-H), 8.52 (dd, *J* = 1.7, 4.8 Hz, 1H, Ar-H), 8.58 (app d, *J* = 2.2 Hz, 1H, Ar-H); ^{13}C NMR (100 MHz, $CDCl_3$) δ 14.02, 20.52, 26.26, 26.31, 26.56, 29.29, 33.26, 33.68, 34.55, 35.90, 51.54, 53.64, 62.71, 67.25, 123.34, 133.48, 137.97, 147.83, 148.81; HRMS (ESI) m/z calculated for $C_{19}H_{33}N_2O$ $[M+H]^+$ 305.2587, found 305.2582; HPLC purity, 95.09%, t_R = 4.36 min.

4.2. Expression and purification of human and *C. albicans* CYP51.

Journal Pre-proofs

The pCWOri+/hCYP51 and pCWOri+/CaCYP51 expression plasmids were a generous gift from Dr. Galina I. Lepesheva (Vanderbilt University School of Medicine, Nashville, Tennessee, USA) [24, 36]. The first eight amino acid residues of both hCYP51 and CaCYP51 constructs were modified to MALLLAVF to optimize expression in *Escherichia coli*. [24, 36, 37] hCYP51 and CaCYP51 were expressed in E. coli strain C43 (DE3) and cells were grown in TB media supplemented with 100 µg/ml ampicillin. After the addition of 2 mM δ-aminolevulinic acid and induction with 1 mM IPTG (Isopropyl β-D1-thiogalactopyranoside), protein expression was carried out at 26°C for 45 h. Isolations and purifications of hCYP51 and CaCYP51 were carried out as described before [21, 38]. For hCYP51 and CaCYP51, expression levels were 300 and 450 nmol/l, respectively. After purification proteins were in a typical cytochrome P450 low-spin state, with a Soret peak at 417 nm. The P450 concentrations were calculated using the extinction coefficient ε417 = 117 mM-1cm-1. The peak in reduced CO difference spectra was at 447 nm for hCYP51 and at 446 nm for CaCYP51 and concentrations were calculated using the extinction coefficient ε450-490 = 91 mM-1cm-1. No inactive form of CYP51 (absorbance maximum at P420) was present in reduced CO difference spectra. Proteins were aliquoted and stored at -70°C.

4.3. UV-Visible Spectra and Specific Ligand Binding.

Apparent dissociation constants (K_D) were measured with spectral titrations to 1 µM CaCYP51 and hCYP51 diluted in 50 mM K-phosphate (pH 7.4), 100 mM NaCl, 0.1 EDTA, 10% glycerol. Ligands were progressively titrated until the maximum spectral responses were reached. For the strongest tight-binding ligands (derivative 24 and 25), titrations were repeated, where P450 concentration was 0.4 µM and titration range was 0.1 – 2 µM. Titration spectra were recorded from 350 to 500 nm with double beam Shimadzu UV-1800 spectrophotometer. Ligands were prepared as DMSO or H_2O stock solutions and added to the sample cuvette with 1 cm optical path length. The same amount of solvent was added to the reference cuvette. Absorbance changes ($\Delta A=A_{max} - A_{min)}$ in difference type II spectra responses were plotted against ligand concentrations and apparent K_D were determined by nonlinear regression in GraphPad Prism 5.04 software. The data were fit to the hyperbola, $\Delta A = \Delta A_{max}$ x [ligand]/(K_D + [ligand]), or to the rearrangement of the Morrison equation (quadratic equation), $\Delta A = \Delta A_{max}$ x (([P450] + [ligand] + K_D) – (([P450] + [ligand] + K_D)^2 - (4 x [P450] x [ligand]))$^{0.5}$)/(2 x [P450]), where tight ligand binding was observed [39]. Each binding assay was repeated three times and the results presented as means ± SD. Absolute

spectra were measured from 350 to 700 nm, which exhibited a red shift in the Soret peak, from ~417 to 421-423, after binding of inhibitors.

4.4. LC-MS based CYP51 inhibition assay.

We developed a quantitatively more precise, considerably cheaper and more convenient CYP51 inhibition assay. Application of LC-MS enabled measurement of concentrations of sterol analytes. The expensive radioactive [3-^{3}H]-lanosterol and scintillation liquid were not required. Each CYP51 reaction mixture was prepared as described for the standard CYP51 inhibition assay, with these changes: concentrations of CaCYP51 and hCYP51 were 0.5 μM and concentration of rat cytochrome P450 reductase (rCPR) was 1.0 μM. 25 μM unlabeled lanosterol was added, 2.5 mM NADPH was used for reaction initiation and the reaction was stopped after 60 min. 15 μM ligand was added for the comparative inhibition assay at the molar ratio enzyme/inhibitor/substrate being 1/30/50. After incubation 200 ng of internal standard lathosterol (99%, D_7) was added to the mixture with the purpose of normalization. The extracted sterols were dissolved in 300 μl methanol and 10 μl was analyzed by HPLC-MS. HPLC (Shimadzu Nexera XR) separation was performed using a PFP(2) 100Å Luna® column 100 × 2 mm, particle size 3μm, (Phenomenex), mobile phase conditions were 80% methanol, 10% H_2O, 10% 1-propanol, 0.05 % formic acid, at a flow rate of 0.25 ml/min. Sterols were selectively detected with MS (Sciex triple quad 3500) with multiple reaction monitoring at 409/191 m/z for lanosterol, 393/214 m/z for FF-MAS and 376/215 m/z for lathosterol (99%, D_7). Retention times for lanosterol, FF-MAS and lathosterol (99%, D_7) were 5.77 min, 5.20 min and 5.14 min, respectively. Lanosterol and FF-MAS concentrations were calculated to the corresponding standard curve. The inhibitory potencies of ligands were compared to CYP51 activity without added ligands and presented as percentage of CYP51 inhibition. Each experiment was repeated three times and the results presented as means ± SD.

4.5. NMR Spectroscopy.

High-resolution NMR spectra were recorded on Bruker Avance Neo 600 MHz and Agilent Technologies VNMRS 800 MHz Spectrometers (NMR Center, National Institute of Chemistry, Slovenia), using cryoprobes, at 25 °C. All the data were collected using the pulse sequences provided in the manufactures' libraries of pulse programs. The residual water signal was suppressed using excitation sculpting [40] and $T_1\rho$ filter of 30 ms was used to

eliminate the background protein resonance. The ^{1}H spectral widths were 8803 and 6250 at 800 and 600 MHz, respectively. NMR samples were prepared in a buffer containing 20 mM (98%, D_{11}), 10% glycerol (99%, D_8), and 100 mM NaCl in D_2O; pD 7.2. All the spectra were recorded at a protein/ligand ratio of 1:100. The protein concentration was 4 μM, and the ligand concentration was 0.4 mM.

The trNOESY [41] spectra were acquired with 4096 data points in t_2, 64 scans, 256 complex points in t_1, and a relaxation delay of 1.5 s. A mixing time from 150 to 350 ms was selected according to the binding affinity of derivatives to compromise between sufficient signal-to-noise and reduced spin diffusion. Adiabatic pulses [42] were applied for the suppression of zero quantum artefacts during the mixing time. Spectra were apodized with a squared sine bell function shifted by π/2 in both dimensions.

The STD ligand epitope mapping experiments [35] were performed with 16.384 data points, a relaxation delay of 5 s, and 1140 scans. The short protein saturation time of 0.3 s was used, selected according to the shortest ligands ^{1}H longitudinal relaxation time (T_1) to avoid the influence of relaxation on STD amplification factors [21, 43]. Selective saturation was achieved by a train of 50 ms long Gauss-shaped pulses separated by 1 ms delay. The on-resonance selective saturation of CYP51 was applied at −0.38 ppm. The off-resonance irradiation was applied at 30 ppm for the reference spectrum. Spectra were zero-filled twice and apodized by an exponential line-broadening function of 3 Hz. Errors in the STD amplification factor were estimated according to the formula: STD amplification factor absolute error = STD amplification factor × $((N_{STD}/I_{STD})^2 + (N_{REF}/I_{REF})^2)1/2$ [44]. N_{STD} and N_{REF} are noise levels in STD and reference spectra. I_{STD} and I_{REF} are signal intensities in STD and reference spectra.

4.6. Molecular Dynamics Simulations.

The starting binding poses for MD simulations of compounds in complex with hCYP51 were derived from the previous calculations [21]. Starting structures of CaCYP51 complexes were produced by docking compounds into the active site of the CaCYP51 crystal structure in complex with azole VT-1161 (PDB entry 5TZ1) [16]. Docking was performed by AutoDock Vina [45]. Conformations with the lowest scoring value and appropriate distance of the pyridine N-atom toward the heme iron (2.0 – 2.2 A) were chosen. Simulations were performed using the GROMACS [46] and CHARMM [47] programs using the periodic boundary conditions and Ewald method for electrostatics according to our previous work [21].

The proper connection between the heme Fe and S atom of Cys449 in hCYP51 and of Cys470 in CaCYP51 was achieved by the correct protonation state of Cys thiol group (thiolate). The MD simulations were run at a constant pressure of 1 bar and temperature 300 K with the time step of 2 fs up to 40 ns. The RMSD of protein backbone calculated over the trajectories showed stabilization of the backbone after 3 ns.

4.7. Anticandidal Activity.

Different strains of *Candida* were used in the study: three clinical isolates (*C. albicans* 475/15, *C. glabrata* 4/6/15, *C. krusei* H1/16) and three reference strains (*C. albicans* ATCC 10231, *C. parapsilosis* ATCC 22019 and *C. tropicalis* ATCC 750). Clinical isolates were obtained by rubbing a sterile cotton swab over oral mucosa from patients at the Ear, Nose, Throat Clinic, Clinical Hospital Centre Zvezdara, Belgrade, Serbia. Strains of *Candida* spp. were determined on CHROMagar plates (Biomerieux, France) and maintained on Sabourand Dextrose Agar (Merck, Germany).

Minimum inhibitory (MIC) were determined by microdilution method in 96 well microtiter plates (EUCAST, 2002) with some modifications [48]. Briefly, fresh yeast cultures were adjusted to a concentration 1.0×10^5 CFU/ well with the use of sterile saline. The microplates with serially diluted compounds were incubated at 37 °C for 24 h. The MIC values were considered as the lowest concentrations without microscopically observed growth after incubation. Commercial antifungal drugs ketoconazole and fluconazole were used as positive controls (Sigma–Aldrich, Germany). The MIC values were measured three times and presented as means ± SD.

4.8. Cytotoxicity Assay.

Human PBMC from healthy blood donors were isolated by density gradient centrifugation with Ficoll-Paque (Pharmacia, Sweden). The cells were cultured in RPMI 1640 (Sigma, Germany) supplemented with 100 U/mL penicillin (Sigma), 100 μg/mL streptomycin (Sigma), 2 mM L-glutamine (Sigma), 50 μM 2-mercaptoethanol (Sigma), and 10% heat-inactivated fetal bovine serum (Gibco, USA).

The PBMCs (100 μL; 1×10^5 cells/mL) were treated with the appropriate vehicle (control cells) and the appropriate concentrations of compounds of interest, in triplicate, in 96-well plates. After 24 h, the metabolic activities were assessed using the CellTiter 96® Aqueous One Solution Cell Proliferation Assay (Promega, Madison, WI, USA), in accordance with the

manufacturer's instructions. The results are expressed as means of triplicates ± SEM of three independent experiments.

ASSOCIATED CONTENT

Supporting Information.

The synthesis scheme of intermediate compounds, expression and purification of Rat cytochrome P450 reductase (rCPR), standard CYP51 inhibition assays, anti-Aspergillus activity, representative UV-visible spectra, representative NMR spectra, and analysis of unrestrained MD simulations.

ACKNOWLEDGEMENTS

This work was supported by the Slovenian Research Agency (Grant No. J1-8145, P1-0010, P1-0390, and P1-0208), Serbian Ministry of Education, Science and Technological Development (Grant No. 451-03-68/2020-14/200007), and by the programme of scientific and technological cooperation between the Republic of Slovenia and the Republic of Serbia (BI-RS/14-15-015). We wish to thank Dr. Galina I. Lepesheva (Vanderbilt University School of Medicine) for the generous gift of the plasmids pCWOri$^+$/hCYP51 and pCWOri$^+$/CaCYP51.

ABBREVIATIONS

CYP51, sterol 14α-demethylase; hCYP51, human CYP51, CaCYP51, *Candida albicans* CYP51; MD, molecular dynamics; K_D, apparent dissociation constants; NOE, nuclear Overhauser effect; trNOESY, transferred NOE spectroscopy; FF-MAS, follicular fluid-meiosis-activating substance; LC-MS, liquid chromatography-mass spectrometry; MIC, minimum inhibitory concentration; MFC, minimum fungicidal concentration; PBMC, peripheral blood mononuclear cells; RMSD, root mean square deviation; STD, saturation transfer difference; HPLC, high-performance liquid chromatography; THF, tetrahydrofuran; HRMS, high resolution mass spectrometry; ESI, electrospray ionization; rCPR, rat cytochrome P450 reductase; IPTG, isopropyl β-*d*-1-thiogalactopyranoside; NADP, nicotinamide adenine dinucleotide phosphate; DLCP, dilaurylphosphatidylcholine; T_1, longitudinal relaxation time.

REFERENCES

[1] G.I. Lepesheva, M.R. Waterman, Sterol 14α-demethylase cytochrome P450 (CYP51), a P450 in all biological kingdoms, Biochim. Biophys. Acta., 1770 (2007) 467-477.

[2] G.I. Lepesheva, M.R. Waterman, Structural basis for conservation in the CYP51 family, Biochim. Biophys. Acta., 1814 (2011) 88-93.

[3] M.R. Waterman, G.I. Lepesheva, Sterol 14α-demethylase, an abundant and essential mixed-function oxidase, Biochem. Biophys. Res. Commun., 338 (2005) 418-422.

[4] G. Lorbek, M. Perse, J. Jeruc, P. Juvan, F.M. Gutierrez-Mariscal, M. Lewinska, R. Gebhardt, R. Keber, S. Horvat, I. Bjorkhem, D. Rozman, Lessons from hepatocyte-specific Cyp51 knockout mice: impaired cholesterol synthesis leads to oval cell-driven liver injury, Sci. Rep., 5 (2015) 8777.

[5] Z. Urlep, G. Lorbek, M. Perse, J. Jeruc, P. Juvan, M. Matz-Soja, R. Gebhardt, I. Bjorkhem, J.A. Hall, R. Bonneau, D.R. Littman, D. Rozman, Disrupting hepatocyte CYP51 from cholesterol synthesis leads to progressive liver injury in the developing mouse and decreases RORC signalling, Sci. Rep., 7 (2017) 40775.

[6] F.R. Santori, P. Huang, S.A. van de Pavert, E.F. Douglass, Jr., D.J. Leaver, B.A. Haubrich, R. Keber, G. Lorbek, T. Konijn, B.N. Rosales, D. Rozman, S. Horvat, A. Rahier, R.E. Mebius, F. Rastinejad, W.D. Nes, D.R. Littman, Identification of natural RORgamma ligands that regulate the development of lymphoid cells, Cell. Metab., 21 (2015) 286-298.

[7] D. Rozman, K. Monostory, Perspectives of the non-statin hypolipidemic agents, Pharmacol. Ther., 127 (2010) 19-40.

[8] D.C. Lamb, D.E. Kelly, M.R. Waterman, M. Stromstedt, D. Rozman, S.L. Kelly, Characteristics of the heterologously expressed human lanosterol 14α-demethylase (other names: P45014DM, CYP51, P45051) and inhibition of the purified human and *Candida albicans* CYP51 with azole antifungal agents, Yeast, 15 (1999) 755-763.

[9] S.C. Chen, T.C. Sorrell, Antifungal agents, Med. J. Aust., 187 (2007) 404-409.

[10] G.I. Lepesheva, L. Friggeri, M.R. Waterman, CYP51 as drug targets for fungi and protozoan parasites: past, present and future, Parasitology, 145 (2018) 1820-1836.

[11] G.I. Lepesheva, H.-W. Park, T.Y. Hargrove, B. Vanhollebeke, Z. Wawrzak, J.M. Harp, M. Sundaramoorthy, W.D. Nes, E. Pays, M. Chaudhuri, F. Villalta, M.R. Waterman, Crystal structures of *Trypanosoma brucei* sterol 14α-demethylase and implications for selective treatment of human infections, J. Biol. Chem., 285 (2010) 1773-1780.

[12] G.I. Lepesheva, T.Y. Hargrove, S. Anderson, Y. Kleshchenko, V. Furtak, Z. Wawrzak, F. Villalta, M.R. Waterman, Structural insights into inhibition of sterol 14α-demethylase in the human pathogen *Trypanosoma cruzi*, J. Biol. Chem., 285 (2010) 25582-25590.

[13] C.K. Chen, S.S. Leung, C. Guilbert, M.P. Jacobson, J.H. McKerrow, L.M. Podust, Structural characterization of CYP51 from *Trypanosoma cruzi* and *Trypanosoma brucei* bound to the antifungal drugs posaconazole and fluconazole, PLoS Negl. Trop. Dis., 4 (2010) 0000651.

[14] N. Strushkevich, S.A. Usanov, H.-W. Park, Structural basis of human CYP51 inhibition by antifungal azoles, J. Mol. Biol., 397 (2010) 1067-1078.

[15] B.C. Monk, T.M. Tomasiak, M.V. Keniya, F.U. Huschmann, J.D. Tyndall, J.D. O'Connell, 3rd, R.D. Cannon, J.G. McDonald, A. Rodriguez, J.S. Finer-Moore, R.M. Stroud,

Architecture of a single membrane spanning cytochrome P450 suggests constraints that orient the catalytic domain relative to a bilayer, Proc. Natl. Acad. Sci. USA, 111 (2014) 3865-3870.

[16] T.Y. Hargrove, L. Friggeri, Z. Wawrzak, A. Qi, W.J. Hoekstra, R.J. Schotzinger, J.D. York, F.P. Guengerich, G.I. Lepesheva, Structural analyses of *Candida albicans* sterol 14α-demethylase complexed with azole drugs address the molecular basis of azole-mediated inhibition of fungal sterol biosynthesis, J. Biol. Chem., 292 (2017) 6728-6743.

[17] T.L. Poulos, B.C. Finzel, A.J. Howard, High-resolution crystal structure of cytochrome P450cam, J. Mol. Biol., 195 (1987) 687-700.

[18] C.C. Lai, C.K. Tan, Y.T. Huang, P.L. Shao, P.R. Hsueh, Current challenges in the management of invasive fungal infections, J. Infect. Chemother., 14 (2008) 77-85.

[19] R. Becher, S.G. Wirsel, Fungal cytochrome P450 sterol 14α-demethylase (CYP51) and azole resistance in plant and human pathogens, Appl. Microbiol. Biotechnol., 95 (2012) 825-840.

[20] T. Korosec, J. Acimovic, M. Seliskar, D. Kocjan, K.F. Tacer, D. Rozman, U. Urleb, Novel cholesterol biosynthesis inhibitors targeting human lanosterol 14α-demethylase (CYP51), Bioorg. Med. Chem., 16 (2008) 209-221.

[21] U. Zelenko, M. Hodoscek, D. Rozman, S. Golic Grdadolnik, Structural insight into the unique binding properties of pyridylethanol(phenylethyl)amine inhibitor in human CYP51, J. Chem. Inf. Model., 54 (2014) 3384-3395.

[22] F.A. Binjubair, J.E. Parker, A.G. Warrilow, K. Puri, P.J. Braidley, E. Tatar, S.L. Kelly, D.E. Kelly, C. Simons, Small-molecule inhibitors targeting sterol 14α-demethylase (CYP51): synthesis, molecular modeling and evaluation against *Candida albicans*, ChemMedChem, 15 (2020) 1294-1309.

[23] A.G. Warrilow, J.E. Parker, D.E. Kelly, S.L. Kelly, Azole affinity of sterol 14α-demethylase (CYP51) enzymes from *Candida albicans* and Homo sapiens, Antimicrob. Agents. Chemother., 57 (2013) 1352-1360.

[24] M. Stromstedt, D. Rozman, M.R. Waterman, The ubiquitously expressed human CYP51 encodes lanosterol 14α-demethylase, a cytochrome P450 whose expression is regulated by oxysterols, Arch. Biochem. Biophys., 329 (1996) 73-81.

[25] T. Korošec, J. Grdadolnik, U. Urleb, D. Kocjan, S. Golič Grdadolnik, Synthesis, conformation, and stereodynamics of a salt of 2-{[2-(3,4-Dichlorophenyl)-ethyl]propylamino}-1-pyridin-3-ylethanol, J. Org. Chem., 71 (2006) 792-795.

[26] T.Y. Hargrove, Z. Wawrzak, P.M. Fisher, S.A. Child, W.D. Nes, F.P. Guengerich, M.R. Waterman, G.I. Lepesheva, Binding of a physiological substrate causes large-scale conformational reorganization in cytochrome P450 51, J. Biol. Chem., 293 (2018) 19344-19353.

[27] T.Y. Hargrove, Z. Wawrzak, F.P. Guengerich, G.I. Lepesheva, A requirement for an active proton delivery network supports a compound I-mediated C-C bond cleavage in CYP51 catalysis, J. Biol. Chem., 295 (2020) 9998-10007.

[28] G.I. Lepesheva, F. Villalta, M.R. Waterman, Targeting *Trypanosoma cruzi* sterol 14*α*-demethylase (CYP51), Adv. Parasitol., 75 (2011) 65-87.

[29] G.I. Lepesheva, M.R. Waterman, Sterol 14α-demethylase (CYP51) as a therapeutic target for human trypanosomiasis and leishmaniasis, Curr. Top. Med. Chem., 11 (2011) 2060-2071.

[30] T.Y. Hargrove, Z. Wawrzak, P.W. Alexander, J.H. Chaplin, M. Keenan, S.A. Charman, C.J. Perez, M.R. Waterman, E. Chatelain, G.I. Lepesheva, Complexes of *Trypanosoma cruzi* sterol 14α-demethylase (CYP51) with two pyridine-based drug candidates for Chagas disease: structural basis for pathogen selectivity, J. Biol. Chem., 288 (2013) 31602-31615.

[31] L. Friggeri, T.Y. Hargrove, Z. Wawrzak, F.P. Guengerich, G.I. Lepesheva, Validation of human sterol 14α-demethylase (CYP51) druggability: structure-guided design, synthesis, and evaluation of stoichiometric, functionally irreversible inhibitors, J. Med. Chem., (2019).

[32] E.P. Gillis, K.J. Eastman, M.D. Hill, D.J. Donnelly, N.A. Meanwell, Applications of fluorine in medicinal chemistry, J. Med. Chem., 58 (2015) 8315-8359.

[33] G.I. Lepesheva, R.D. Ott, T.Y. Hargrove, Y.Y. Kleshchenko, I. Schuster, W.D. Nes, G.C. Hill, F. Villalta, M.R. Waterman, Sterol 14α-demethylase as a potential target for antitrypanosomal therapy: enzyme inhibition and parasite cell growth, Chem. Biol., 14 (2007) 1283-1293.

[34] L. Friggeri, T.Y. Hargrove, G. Rachakonda, A.D. Williams, Z. Wawrzak, R. Di Santo, D. De Vita, M.R. Waterman, S. Tortorella, F. Villalta, G.I. Lepesheva, Structural basis for rational design of inhibitors targeting *Trypanosoma cruzi* sterol 14α-demethylase: two regions of the enzyme molecule potentiate its inhibition, J. Med. Chem., 57 (2014) 6704-6717.

[35] M. Mayer, B. Meyer, Group epitope mapping by saturation transfer difference NMR to identify segments of a ligand in direct contact with a protein receptor, J. Am. Chem. Soc., 123 (2001) 6108-6117.

[36] G.I. Lepesheva, L.M. Podust, A. Bellamine, M.R. Waterman, Folding requirements are different between sterol 14α-demethylase (CYP51) from *Mycobacterium tuberculosis* and human or fungal orthologs, J. Biol. Chem., 276 (2001) 28413-28420.

[37] H.J. Barnes, M.P. Arlotto, M.R. Waterman, Expression and enzymatic activity of recombinant cytochrome P450 17 α-hydroxylase in *Escherichia coli*, Proc. Natl. Acad. Sci. USA, 88 (1991) 5597-5601.

[38] T. Režen, I. Ogris, M. Sever, F. Merzel, S. Golič Grdadolnik, D. Rozman, Evaluation of Selected CYP51A1 Polymorphisms in view of interactions with substrate and redox partner, Front Pharmacol, 8 (2017) 417.

[39] A.G. Warrilow, C.M. Martel, J.E. Parker, N. Melo, D.C. Lamb, W.D. Nes, D.E. Kelly, S.L. Kelly, Azole binding properties of *Candida albicans* sterol 14-α demethylase (CaCYP51), Antimicrob. Agents. Chemother., 54 (2010) 4235-4245.

[40] T.L. Hwang, A.J. Shaka, Water suppresion that works. Excitation sculpting using arbitrary wave-forms and pulsed-field gradients, J. Magn. Res., 112 (1995) 275-279.

[41] G.M. Clore, A.M. Gronenborn, Theory and applications of the transferred nuclear overhauser effect to the study of the conformations of small ligands bound to proteins, J. Magn. Res., 48 (1982) 402-417.

[42] M.J. Thrippleton, J. Keeler, Elimination of zero-quantum interference in two-dimensional NMR spectra, Angew. Chem. Int. Ed. Engl., 115 (2003) 4068-4071.

[43] J. Yan, A.D. Kline, H. Mo, M.J. Shapiro, E.R. Zartler, The effect of relaxation on the epitope mapping by saturation transfer difference NMR, J. Magn. Res., 163 (2003) 270-276.

[44] C. McCullough, M. Wang, L. Rong, M. Caffrey, Characterization of influenza hemagglutinin interactions with receptor by NMR, PLoS ONE, 7 (2012) e33958.

[45] O. Trott, A.J. Olson, AutoDock Vina: Improving the speed and accuracy of docking with a new scoring function, efficient optimization, and multithreading, J. Comput. Chem., 31 (2010) 455-461.

[46] M.J. Abraham, T. Murtola, R. Schulz, S. Pall, J.C. Smith, B. Hess, E. Lindahl, High performance molecular simulations through multi-level parallelism from laptops to supercomputers., SoftwareX, 1-2 (2015) 19-25.

[47] B.R. Brooks, C.L. Brooks, 3rd, A.D. Mackerell, Jr., L. Nilsson, R.J. Petrella, B. Roux, Y. Won, G. Archontis, C. Bartels, S. Boresch, A. Caflisch, L. Caves, Q. Cui, A.R. Dinner, M. Feig, S. Fischer, J. Gao, M. Hodoscek, W. Im, K. Kuczera, T. Lazaridis, J. Ma, V. Ovchinnikov, E. Paci, R.W. Pastor, C.B. Post, J.Z. Pu, M. Schaefer, B. Tidor, R.M. Venable, H.L. Woodcock, X. Wu, W. Yang, D.M. York, M. Karplus, CHARMM: the biomolecular simulation program, J. Comput. Chem., 30 (2009) 1545-1614.

[48] M. Smiljkovic, M.T. Matsoukas, E. Kritsi, U. Zelenko, S. Golic Grdadolnik, R.C. Calhelha, I. Ferreira, S. Sankovic-Babic, J. Glamoclija, T. Fotopoulou, M. Koufaki, P. Zoumpoulakis, M. Sokovic, Nitrate esters of heteroaromatic compounds as *Candida albicans* CYP51 enzyme inhibitors, ChemMedChem, 13 (2018) 251-258.

Journal Pre-proofs

Highlights

- Pyridylethanol(phenylethyl)amines inhibited *Candida albicans* CYP51.
- Their binding mode was determined by NMR and molecular dynamics simulations.
- Structural requirements for selectivity over human orthologue were determined.
- Potent, highly selective CaCYP51 inhibitors were designed and synthesized.
- A structurally distinct, non-azole lead for development of antifungals was provided.

Journal Pre-proofs

Declaration of interests

☒ The authors declare that they have no known competing financial interests or personal relationships that could have appeared to influence the work reported in this paper.

☐The authors declare the following financial interests/personal relationships which may be considered as potential competing interests:

Journal Pre-proofs